TURUN YLIOPISTON JULKAISUJA
ANNALES UNIVERSITATIS TURKUENSIS

SARJA - SER. D OSA - TOM. 1016

MEDICA - ODONTOLOGICA

THE POSSIBILITIES AND DOSIMETRIC LIMITATIONS OF MLC-BASED INTENSITY-MODULATED RADIOTHERAPY DELIVERY AND OPTIMIZATION TECHNIQUES

by

Jan Seppälä

TURUN YLIOPISTO
UNIVERSITY OF TURKU
Turku 2012

From Department of Oncology and Radiotherapy, University of Turku, Turku, Finland
and
Cancer Center, Kuopio University Hospital, Kuopio, Finland

Supervised by

Docent Jarmo Kulmala, Ph.D.
Department of Oncology and Radiotherapy
University of Turku, Finland

and

Docent Tapani Lahtinen, Ph.D.
Cancer Center
Kuopio University Hospital, Finland

and

Professor Heikki Minn, M.D., Ph.D.
Department of Oncology and Radiotherapy
University of Turku, Finland

Reviewed by

Docent Mikko Tenhunen, Ph.D.
Department of Oncology
Helsinki University Central Hospital, Finland

and

Adjunct Professor Anders Ahnesjö, Ph.D.
Department of Radiology, Oncology and Radiation Sciences
Uppsala University, Sweden

Dissertation Opponent

Chief Physicist, Håkan Nyström, Ph.D.
Skandion Clinic
Uppsala, Sweden

ISBN 978-951-29-5035-5 (PRINT)
ISBN 978-951-29-5036-2 (PDF)
ISSN 0355-9483
Painosalama Oy – Turku, Finland 2012

To Anton, Emil and Kati

ABSTRACT

Jan Seppälä
THE POSSIBILITIES AND DOSIMETRIC LIMITATIONS OF MLC-BASED INTENSITY-MODULATED RADIOTHERAPY DELIVERY AND OPTIMIZATION TECHNIQUES
Department of Oncology and Radiotherapy, University of Turku, Turku, Finland
Annales Universitatis Turkuensis, 2012

The use of intensity-modulated radiotherapy (IMRT) has increased extensively in the modern radiotherapy (RT) treatments over the past two decades. Radiation dose distributions can be delivered with higher conformality with IMRT when compared to the conventional 3D-conformal radiotherapy (3D-CRT). Higher conformality and target coverage increases the probability of tumour control and decreases the normal tissue complications. The primary goal of this work is to improve and evaluate the accuracy, efficiency and delivery techniques of RT treatments by using IMRT.

This study evaluated the dosimetric limitations and possibilities of IMRT in small (treatments of head-and-neck, prostate and lung cancer) and large volumes (primitive neuroectodermal tumours). The dose coverage of target volumes and the sparing of critical organs were increased with IMRT when compared to 3D-CRT. The developed split field IMRT technique was found to be safe and accurate method in craniospinal irradiations. By using IMRT in simultaneous integrated boosting of biologically defined target volumes of localized prostate cancer high doses were achievable with only small increase in the treatment complexity. Biological plan optimization increased the probability of uncomplicated control on average by 28% when compared to standard IMRT delivery.

Unfortunately IMRT carries also some drawbacks. In IMRT the beam modulation is realized by splitting a large radiation field to small apertures. The smaller the beam apertures are the larger the rebuild-up and rebuild-down effects are at the tissue interfaces. The limitations to use IMRT with small apertures in the treatments of small lung tumours were investigated with dosimetric film measurements. The results confirmed that the peripheral doses of the small lung tumours were decreased as the effective field size was decreased. The studied calculation algorithms were not able to model the dose deficiency of the tumours accurately. The use of small sliding window apertures of 2 mm and 4 mm decreased the tumour peripheral dose by 6% when compared to 3D-CRT treatment plan.

A direct aperture based optimization (DABO) technique was examined as a solution to decrease the treatment complexity. The DABO IMRT technique was able to achieve treatment plans equivalent with the conventional IMRT fluence based optimization techniques in the concave head-and-neck target volumes. With DABO the effective field sizes were increased and the number of MUs was reduced with a factor of two. The optimality of a treatment plan and the therapeutic ratio can be further enhanced by using dose painting based on regional radiosensitivities imaged with functional imaging methods.

Keywords: Intensity-modulated radiotherapy, direct aperture based optimization, split field IMRT, biological dose optimization

TIIVISTELMÄ

Jan Seppälä
MONILIUSKAKOLLIMAATTOREILLA OHJATUN INTENSITEETTI-MUOKATUN SÄDEHOIDON TOTEUTTAMIS- JA OPTIMOINTITEKNIIKOIDEN MAHDOLLISUUDET SEKÄ DOSIMETRISET RAJOITUKSET
Syöpätaudit ja sädehoito, Turun yliopisto, Turku.
Annales Universitatis Turkuensis, 2012

Intensiteettimuokatun sädehoidon (IMRT) käyttö on lisääntynyt modernissa sädehoidossa kahden viime vuosikymmenen aikana. IMRT:llä säteilyn annosjakaumia voidaan muokata kohdealueita myötäileviksi, jolloin tervekudoksia saadaan säästettyä paremmin kuin perinteisellä 3D-konformaalisella sädehoidolla (3D-CRT). Kaikkia IMRT:n etuja ei ole kuitenkaan vielä hyödynnetty sädehoidon toteutuksessa ja toisaalta tietoa IMRT:n rajoitteista erikokoisten kohdealueiden hoidoissa on liian vähän. Tämän työn tavoitteena oli parantaa sädehoidon tarkkuutta ja tehokkuutta uusilla IMRT-sovelluksilla sekä arvioida tekniikoiden dosimetrisia rajoituksia.

Väitöskirjatyössä tutkittiin IMRT-tekniikan mahdollisuuksia ja rajoituksia pään ja kaulan alueen, eturauhasen, keuhkojen alueen ja kraniospinaalisädetysten hoidoissa. IMRT:llä saavutettiin hoitokohteisiin parempi annoskattavuus kuin 3D-CRT-tekniikalla vaikka tervekudosten annokset pienenivät. IMRT mahdollisti kranio-spinaalisädetystysten turvallisemman toteuttamisen parantunein kohdeannoksin. IMRT:n hyödyntämistä säteilylle vastustuskykyisempien biologisten kohdealueiden annosmaalauksessa tutkittiin eturauhassyöpäpotilaiden ulkoisessa sädehoidossa. Biologisesti kohdennetuilla IMRT-annossuunnitelmilla saavutettiin laskennallisesti parempi kasvainkontrolli pienentyneellä tervekudostoksisuudella. Tautivapaan ajan todennäköisyys ilman hoidosta aiheutuneita sivuvaikutuksia parani 28 % uudella IMRT-tekniikalla verrattaessa sitä perinteiseen IMRT-hoitojen toteutukseen.

IMRT:n toteuttaminen vaatii pieniä säteilyn osakenttiä ja hoitokoneiden sädetysaika (MU-määrä) lisääntyy. Tämä puolestaan lisää hoitoaikoja ja haitallista siroavan säteilyn määrää. Pienten kenttien dosimetria on annoslaskenta-algoritmeille haastavaa ja mitatun ja lasketun annoksen välillä syntyy helposti suuria eroja. Annoslaskenta-algoritmien tarkkuutta keuhkojen alueella tutkittiin pienillä IMRT-kentillä filmimittauksin. Tulokset osoittivat, että tutkitut annoslaskenta-algoritmit eivät kykene mallintamaan pienten IMRT-kenttien tuottamia annoksia keuhkotuumoreihin tarkasti. Suurimmat virheet annoksien epätarkkuuksissa havaittiin tuumorien reuna-alueilla.

IMRT-hoitojen tehokkuutta voidaan parantaa moniliuskakollimaattoreiden (MLC) suoralla optimoinnilla (DABO). DABO-tekniikalla optimoidut säteilykentät eivät vaadi pieniä liuskarakoja hoitojen toteutuksessa joten hoidot ovat laskennallisesti sekä toteutuksellisesti tarkempia. Lisäksi vähentyneiden MU-määrien takia siroavan säteilyn määrä pienenee. Työssä tutkitulla suoralla optimointitekniikalla saavutettiin perinteisiä IMRT-tekniikoita vastaavat annosjakaumat kaksi kertaa pienemmillä MU-lukemilla. Hoitosuunnitelmien optimaalisuutta ja terapeuttista hyötyä voidaan edelleen parantaa käyttämällä annosmaalausta säteilylle vastustuskykyisimpiin alueisiin.

Avainsanat: Intensiteettimuokattu sädehoito (IMRT), suora optimointi, jaettujen kenttien IMRT, biologinen annoksen optimointi

TABLE OF CONTENTS

ABBREVIATIONS

3D-CRT	3-dimensional conformal radiotherapy
α/β	Tissue and tumour specific term in linear quadratic formula, which describes the curvature of a cell survival curve
AAA	Anisotropic analytic algorithm
ACE	[^{11}C]acetate
BEV	Beam's eye view
BTV	Biologically defined target volume
CCC	Collapsed cone convolution
CSI	Craniospinal irradiation
CT	X-ray computed tomography
CTV	Clinical target volume
D95	The minimum dose covering 95% of the PTV
DABO	Direct aperture based optimization
DLS	Dosimetric leaf separation
DMLC	Dynamic IMRT delivery technique
DPBC	Dose painting by contours
DPBN	Dose painting by numbers
DVH	Dose volume histogram
EBRT	External beam radiotherapy
EPID	Electronic portal imaging device
EUD	Equivalent uniform dose
FDG	[^{18}F]fluoro-2-deoxy-glucose
gEUD	Generalized equivalent uniform dose
GTV	Gross tumour volume
H&N	Head-and-neck
HD-MLC	High-definition multileaf collimator
IMAT	Intensity-modulated arc therapy
IMRT	Intensity-modulated radiotherapy
IPL	Intraprostatic lesion
L-BFGS-B	Limited memory variant of the Broyden–Fletcher–Goldfarb–Shanno algorithm
LKB-model	Lyman-Kutcher-Burman normal tissue complication probability model
LMC	Leaf motion calculator
LQ	Linear-quadratic
MC	Monte Carlo
MLC	Multileaf collimator
MOSFET	Metal oxide semiconductor field effect transistor

MR	Magnetic resonance
MRI	Magnetic resonance imaging
MRS	Magnetic resonance spectroscopy
MU	Monitor unit
NSCLC	Non-small cell lung cancer
NTCP	Normal tissue complication probability
OAR	Organ at risk
PBC	Pencil beam convolution
PCa	Prostate cancer
PET	Positron emission tomography
PET/CT	Combined PET and CT
PMMA	Polymethyl methacrylate
PNET	Primitive neuroectodermal tumour
PTV	Planning target volume
PUC	Probability of uncomplicated control
PVE	Partial volume effect
RT	Radiotherapy
SBRT	Stereotactic body radiotherapy
SD	Standard deviation
sfIMRT	Split field intensity-modulated radiotherapy
SIB	Simultaneous integrated boost
sIMRT	Standard intensity-modulated radiotherapy
SLRT	Stereotactic lung radiotherapy
SMLC	Segmental IMRT delivery technique
SWA	Sliding window aperture
T&G	Tongue and groove
TCP	Tumour control probability
TLD	Thermoluminescent dosimeter
TPS	Treatment planning system
TR	Tolerance range
VMAT	Volumetric modulated arc treatment
ZM-model	TCP model based on Zaider and Minerbo

LIST OF ORIGINAL PUBLICATIONS

This thesis is based on the following articles, which are referred to in the text by their Roman numerals (I–IV).

I Seppälä J, Kulmala J, Lindholm P, Minn H. A method to improve target dose homogeneity of craniospinal irradiation using dynamic split field IMRT. *Radiother Oncol*. 96:209-215, 2010.

II Seppälä J, Suilamo S, Kulmala J, Mali P, Minn H. A dosimetric phantom study of dose accuracy and build-up effects using IMRT and RapidArc in stereotactic irradiation of lung tumours. *Radiat Oncol*. In Press.

III Seppälä J, Lahtinen T, Kolmonen P. Major reduction of monitor units with the avoidance of leaf-sequencing step by direct aperture based IMRT optimisation. *Acta Oncol*, 48:426-430, 2009.

IV Seppälä J, Seppänen M, Arponen E, Lindholm P, Minn H. Carbon-11 acetate PET/CT based dose escalated IMRT in prostate cancer. *Radiother Oncol*, 93:234-240, 2009.

1 INTRODUCTION

The aim of radiotherapy (RT) is to deliver radiation doses sufficient to eradicate all the tumour cells with as low normal tissue damage as possible. The tumour response to RT depends mainly on the delivered dose, but the biological effect is also influenced by treatment fractionation, total treatment time, individual radiosensitivity, oxygenation of the tissue, radiosensitivity of different cells, damage repair of the irradiated cells and tumour microenvironment and repopulation (Halperin et al 2007, Ling et al 2000, Speight and Roach 2007). The irradiation of normal tissues is unavoidable when delivering high doses of radiation to tumour cells. The amount of damage to different organs depends also on the absolute dose, the volume irradiated, the radiation response of an organ and an individual patient (Bentzen et al 2010). The tolerance of normal tissues to radiation is the main dose limiting factor and thus in many cases the main limiting factor for the local control of disease.

RT treatment planning starts by identifying the potential areas of clonogenic tumour cells. Different imaging methods can be used and the most common is X-ray computed tomography (CT). With CT the patient anatomy can be visualized with high geometric accuracy and the electron density of the patient can be approximated and consequently the radiation dose can be calculated with adequate accuracy. Technical improvements in different imaging methods, like positron emission tomography (PET) and magnetic resonance imaging (MRI), have greatly improved the ability to identify the areas of tumour spread and critical normal structures.

The imaged and contoured target volumes can be highly concave and located near critical and radiosensitive organs. With 3-dimensional conformal radiotherapy (3D-CRT) the dose distributions can not be sculpted to the concave shapes of the targets and as a consequence a part of the normal tissues are exposed to high doses of radiation. Intensity-modulated radiotherapy (IMRT) has improved the conformality of radiation dose delivery. In IMRT the treatment planning process is realized by inverse problem where the goals and limits of radiation dose are set to the defined target volumes and critical organs. IMRT plan optimization searches for the radiation beam intensity maps that can be physically delivered to create the optimal dose distribution to each patient. IMRT is able to deliver concave dose distributions allowing better tumour volume coverage and normal tissue sparing when compared to the 3D-CRT (Arbea et al 2010, Cozzi et al 2004, Fenoglietto et al 2008).

IMRT has been recognized as the best delivery method of external beam radiotherapy (EBRT) with conventional linear accelerators (Cahlon et al 2008, Wu 2000, Zelefsky et al 2000). However, the full potential of IMRT has not been solidified in the variety of radiotherapy treatments. For example, the treatments of craniospinal irradiation (CSI) having very large treatment volumes are typically realized with a variety of 3D-CRT techniques (Koshy et al 2004, Michalski et al 2002, South et al 2008, Verellen

et al 1996). The 3D-CRT delivery techniques in CSI are usually based on geometrical matching of divergent radiation beams. As a consequence the accuracy of the treatments is very sensitive to geometrical inaccuracies in treatment delivery. In addition, the dose coverage and the sparing of critical organs are not optimal with the 3D-CRT techniques.

Unfortunately the use of IMRT decreases the effective aperture sizes when compared to conventional 3D-CRT. By decreasing the effective field size the rebuild-up and rebuild-down effects are increased in the lung-tumour interfaces potentially decreasing the dose coverage of the tumour. All dose calculation algorithms used in radiotherapy are not able to model the small field electron transport in heterogeneities with high accuracy and consequently the calculation accuracy can be compromised at the interface areas (Ahnesjö et al 1999, Tomé et al 2002). This becomes a clinical concern if IMRT is used for the treatments of small lung tumours. The dosimetric accuracy of IMRT has not been extensively studied with small aperture sizes in heterogeneous volumes. Still the modulated delivery methods are proposed as the best approaches for the dose delivery of the small tumours of stereotactic lung radiotherapy (SLRT) (McGrath et al 2010, Verbakel et al 2009, Videtic et al 2010).

Most IMRT optimization methods are realized by first optimizing the radiation intensity map (fluence) for each beam. This is followed by an optimization to find the allowed and optimal shapes of the multileaf collimator (MLC). Because of the separation of intensity optimization and leaf optimization, a large number of complex and narrow MLC shapes are needed. This will not only lead to an increase in the monitor units (MU) needed to deliver the prescription dose but also decreases the size of the apertures and increases the duration of the treatments. Direct aperture based optimization (DABO) could be one solution to improve the efficiency of the treatments by reducing the number of MUs and increasing the effective field size of the treatment. Consequently the IMRT treatments would be less volatile to MLC positioning errors and calculation inaccuracies.

The clinical optimization of IMRT treatment fields is currently based on the physical quantities such as dose and volume. Current clinical approach is to deliver a uniform dose distribution to the defined target volume(s). This uniform dose approach does not, however, give the highest possible tumour control probability (TCP) if there are different radiosensitivities within the target volume(s). New functional imaging methods, such as PET and MRI have the possibility to identify areas of different radiosensitivities. Molecular imaging based treatment plan optimization accounting for the variability in radiation sensitivity could have the potential to design the dose distributions to obtain higher TCP with decreased normal tissue complication probability (NTCP).

2 AIMS

IMRT has become a standard technique in RT and gradually replaced conventional 3D-CRT in various treatment regions. Nevertheless, there are conditions where the possibilities and dosimetric limitations of IMRT have not been extensively evaluated. Therefore, the purpose of this study was

- to explore the feasibility of IMRT in small and large treatment volumes
- to evaluate the dosimetric accuracy of small IMRT field apertures and to investigate the effect of narrow apertures to the surface doses of lung tumours
- to study the impact of direct aperture based optimization on the efficiency of IMRT by means of monitor unit reduction and increase of the effective aperture sizes
- to increase the TCP and decrease the normal tissue toxicity by using molecular imaging based treatment plan optimization

3 INTENSITY-MODULATED RADIOTHERAPY (IMRT)

3.1 From 3D-CRT to IMRT

In 3D-CRT the dose from external beam radiation is determined in 3D-patient geometry. The patient geometry is usually imaged by CT and the reconstructed transverse images are used to delineate the planning target volumes (PTV) and organs at risk (OAR). The target volume(s) usually comprises the bulk of the tumour, the tumour spread visualized by different imaging methods and areas at risk of tumour spread. Treatment planning in 3D-CRT is performed by setting multiple radiation beams to conform the tumour shape with MLCs that consist of two sets of opposed, usually 40 or 60, leaf pairs. MLCs are also used to limit the exposure to nearby normal tissues and critical organs. The radiation beam directions are usually set by the aid of beams "eye" view (BEV) where the delineated volumes of interest are visualized from the beams perspective. Radiation dose in the patient from the fixed beams is calculated in transverse planes of the images and the resulting dose distribution can be visualized in 3D. Volumetric dose calculations and volumetric plan evaluation tools like dose volume histograms (DVH) of the delineated structures are used to evaluate the plan quality. If the discrepancy between the desired dose and the calculated dose is unacceptable, then the number of beams, beam weighting, energy or directions is changed. The process is repeated until the treatment plan meets the criteria set. The resulting dose distribution in patient is therefore planned by "forward planning" in a trial and error fashion.

IMRT is basically an extension of 3D-CRT where the dose is delivered by non-uniform beam intensities. The uniform beam intensity across the treatment field of 3D-CRT and the non-uniform beam intensity of IMRT are illustrated in Figure 3-1. In IMRT the non-uniform radiation intensity of an individual beam is optimized by using inverse planning (Brahme 1988). Thus a reverse approach is taken to find the best possible solution for a given target volume and critical organs. IMRT treatment planning process is usually completed in three separate steps: 1) Optimal radiation fluence pattern is optimized for each treatment field based on the user defined dose volume constraints. 2) Leaf motion calculator (LMC) optimizes the patterns of MLC apertures from the optimized fluences by considering the physical and dosimetrical properties of the MLC. 3) The deliverable MLC field apertures are converted to 2D-fluence distribution from which the dose calculation engine performs the actual dose calculation.

IMRT has replaced conventional 3D-CRT as a routine technique in treatment of several cancers. The dosimetric advantage of IMRT over 3D-CRT is obvious in terms of sparing of critical organs, dose coverage and homogeneity of PTV (Cozzi et al 2004, Fenoglietto et al 2008, Gomez et al 2010, Jabbari et al 2005, Vergeer et al 2009). Not only has IMRT reduced the toxicity of the given treatments but also the sparing of OARs below the tolerance limits has enabled dose escalation of the target volumes and consequently

increased the TCP (Alongi et al 2009, Palma et al 2008, Stewart et al 2009). The differences in dose distribution of 3D-CRT and IMRT have translated into a significant improvement in quality of life (Jabbari et al 2005, Nutting et al 2011, Vergeer et al 2009).

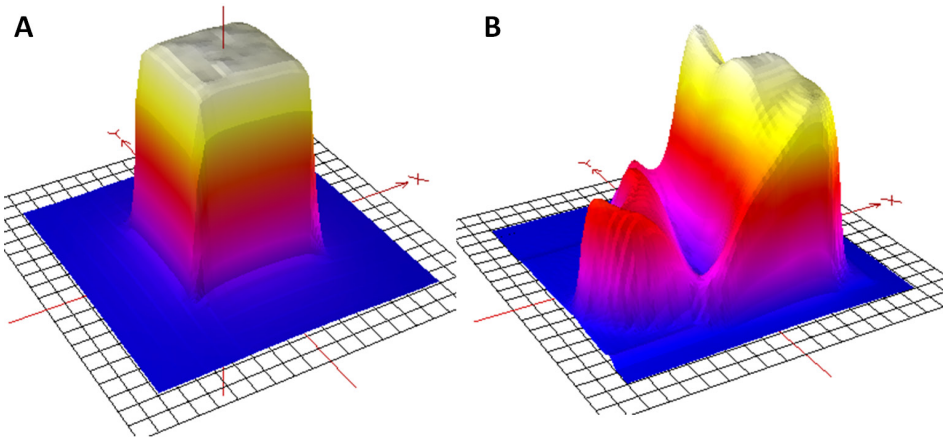

Figure 3-1. An example of radiation beam intensities of an individual external beam of 3D-CRT (A) and IMRT (B).

IMRT treatment delivery is composed of multiple small apertures and to deliver the prescription dose to the patient the amount of MUs is increased. The increased number of MUs needed to deliver a desired dose to the target volume increases the treatment delivery times and increases the amount of scattered radiation from the collimators and head leakage. The decrease in beam aperture sizes has also emphasized the importance of MLC dosimetric parameters used in treatment planning systems (TPS) and consequently the decrease in effective aperture sizes can create inaccuracies in dose calculation (LoSasso et al 1998).

3.2 MLC based delivery methods of IMRT

The optimized non-uniform IMRT radiation fluence has been realized with fabricated compensators (Chang et al 2004), binary leaf openings (Oldham and Webb 1997, Salter 2001) or even only by the secondary collimators (Earl et al 2007). However, the most common technique is to use the MLCs of the treatment unit to convert the optimized intensity distributions to deliverable radiation beam intensities. MLC consists of multiple computer controlled leaves that can be individually moved to shape the beam. In Figure 3-2 is an example of one commercial MLC design. IMRT can be delivered with MLC by either in dynamic mode (DMLC) or in segmental mode (SMLC). In DMLC the leaves are moving continuously during the beam on time and in SMLC delivery the radiation is turned off while the aperture shapes will cycle. The dynamic or static shapes of the MLC will form the optimized radiation fluence or will be optimized in the case of DABO.

Every MLC leaf position has its own control point data. The number of control points in dynamic dose delivery is usually between 20 to 60. These data are stored in a file and acts as an input data for the MLC control system. The perfect MLC for the IMRT delivery would include good mechanical accuracy, small radiation beam penumbra, minor leaf leakage and fine leaf width. High maximum leaf speed and leaf acceleration are also preferable for the precise DMLC delivery. Leaf design also affects the dose calculation accuracy by the means of tongue and groove effect (T&G), transmission through rounded leaf ends and the transmission and scattering properties of the MLC.

In the SMLC dose delivery each static field consists of a number of beamlets, some of which may be very small. The use of SMLC requires that the optimized fluence can be approximated by discrete levels of intensity. The ability of SMLC to deliver the optimized fluence depends on the number of intensity levels used and the spatial resolution of the MLC (Chui et al 2001). The larger the number of intensity levels or apertures is in SMLC the closer the dose distribution is to the dose delivered with DMLC. With 10-20 apertures or more within one field the SMLC and DMLC produce dosimetrically comparable results (Agazaryan and Solberg 2003, Longobardi et al 2005). However, the greater the intensity levels are the higher number of static MLC apertures is created consequently decreasing the field size of the apertures.

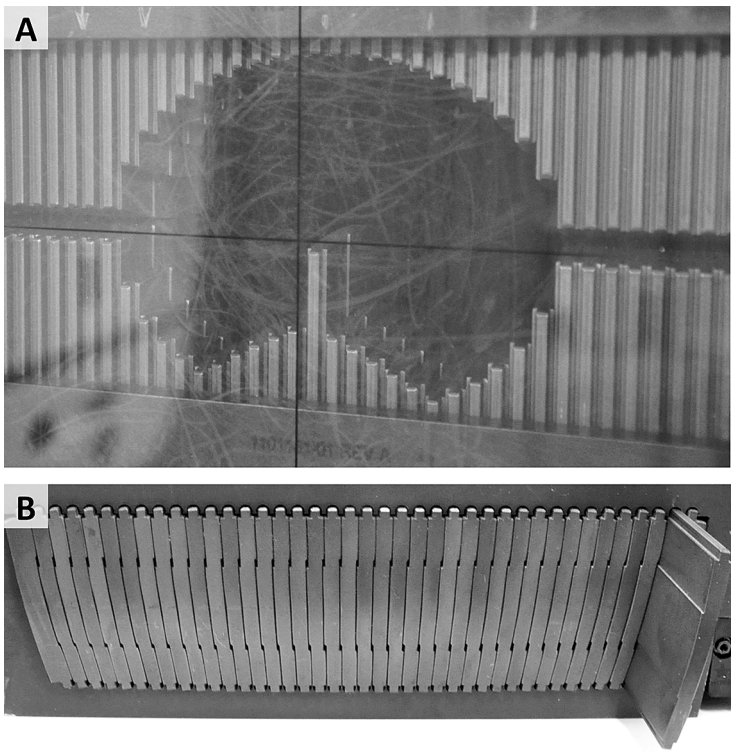

Figure 3-2. The design of the 80-leaf Varian MLC (Varian Medical Systems, Palo Alto, CA) with rounded leaf ends (A). The MLC-model has a tongue and groove construction to minimize interleaf leakage and the leaf sides follow the beam divergence (B).

In DMLC the dose rate and the speed of the leaves are continuously adjusted by the computer controlled MLC system during the beam on time. The advantage of DMLC is its ability to deliver the radiation with continuous movement of the leaves resulting treatment delivery times about 15% shorter than with the SMLC delivery method (Alaei et al 2004, Nicolini et al 2005). However, MUs required to deliver the dose distribution to the patient is 20% higher with the DMLC (Alaei et al 2004, Chui et al 2001). With DMLC the target coverage and critical organ protection has been reported to be slightly better than with SMLC (Chui et al 2001, Nicolini et al 2005).

A recent technical development in radiation delivery is the volumetric modulated arc therapy (VMAT) or intensity-modulated arc therapy (IMAT) or RapidArc in the case of Varian treatment machines. The technique with dynamic MLCs and moving gantry was first proposed by Yu in 1995. VMAT uses continuous gantry angle rotation and at the same time the shapes of the apertures and the dose rate of the treatment machine are varied. VMAT reduces the treatment time by a factor of 8 to 2 by using single or two rotations (arcs), respectively when compared to seven field IMRT treatment plans (Clivio et al 2009, Sze et al 2011, Vieillot et al 2010). In complex treatments with concave target volumes, the VMAT needs usually at least two or three arcs to be dosimetrically equivalent to fixed gantry IMRT treatments (Guckenberger et al 2009, Vanetti et al 2009, Wu et al 2009, Yoo et al 2010). However, with circular target volumes, like prostate cancer, one arc has been found to be adequate to achieve comparable dose distributions to conventional IMRT (Fontenot et al 2011). The number of MUs has also been decreased by a factor of 2-4 by using VMAT techniques when compared to fixed gantry IMRT techniques (Lee et al 2011, Teoh et al 2011).

By reducing high dose areas of normal tissues the VMAT technique delivers lower doses to a greater patient volume when compared to fixed gantry IMRT techniques. Volume of low doses under 5 Gy is almost doubled with VMAT when compared to standard IMRT techniques (Guckenberger et al 2009, Ong et al 2010, Wiezorek et al 2011) as the integral dose and volume receiving low doses are equal with SMLC and DMLC (Jothybasu et al 2009).

3.3 The inverse problem of IMRT

Although intensity modulation can be achieved through forward planning, the large number of parameters makes the task difficult, especially for complex cases where concave target volumes are located near critical organs. In IMRT the intensity distributions are modelled as an inverse problem. A variety of algorithms have been developed to deliver a required radiation dose to the PTV while minimizing the dose to normal tissues by the inverse problem (Chui and Spirou 2001, Kolmonen et al 1998, Li et al 2003, Zhang et al 2004). Not only have the physical or biological limitations of the irradiated organs to be accounted for in the optimization but also the mechanical limitations of the radiotherapy delivery system.

In IMRT the dose distributions are optimized by using an objective function or cost function. Objective function is usually based on the user defined dose limits of the OAR and the prescription dose(s) of the target volume(s) and the corresponding weighting factors. The objective function relates the actual dose distribution to a desirable dose distribution. In the inverse planning of IMRT the objective function is commonly minimized by optimizing the beam intensity distributions.

Every optimization algorithm requires iterative dose calculations, and generally a high number of iterations are required to achieve an optimal plan. Typically, each iteration involves changing the boundary conditions using the search algorithm and recalculating the dose distribution. Simplified dose calculation methods are often used in the dose optimization to speed up the optimization process. This might have some consequences for doses of critical structures or dose coverage of the PTV (Siebers et al 2001).

The most applied device in shaping of field intensity is the MLC. MLCs can be controlled precisely to provide increments of the dose delivery sequence. In most common optimizations a set of fluence maps are optimized for each field and a separate leaf sequencing algorithm is used to transform the fluence distributions into deliverable MLC apertures. The leaf sequencing algorithms takes into account the given mechanical limitations of the MLCs and the physical properties of the MLCs, such like leaf transmission factors, dosimetric leaf separation (DLS) and so-called tongue and groove (T&G) corrections. The number of MLC control points has to always be greater or equal to the number of intensity levels of the beam. The increase in MUs required to deliver the modulated field depends on the complexity of the field intensity and the number of intensity levels. The final dose distribution is calculated from fluence distributions generated from the actual leaf positions. Depending on dose calculation algorithm this could create inaccuracies in the dose calculation within and near inhomogeneities since the loss of lateral electron fluence by the use of small field sizes is not correctly accounted.

3.4 IMRT optimization strategies

IMRT optimization algorithms can be divided into fluence or aperture based optimizations. In fluence based optimization the optimal fluence for each field is determined and converted to deliverable movements or segments of the MLC. In aperture based optimization the apertures are optimized directly without any leaf sequencing algorithm. Both optimization strategies need an objective function to determine the quality of the treatment plan with user defined limitations. The objective function can be determined by the usual physical and volume based constraints. The use of biological objective functions has been described to enhance the dose distributions in the patients (Qi et al 2009, Semenenko et al 2008).

The IMRT optimization functions have many variables and as a result a large number of local minimum and maximum can be found. Finding a global minimum is challenging and

impossible to solve if the critical demands are too restrictive. Deterministic optimization methods, like gradient, conjugate gradient and maximum likelihood methods, are most commonly implemented in the commercial TPSs since they need less iteration to obtain a practical solution (Zhang et al 2004). The deterministic optimization process can, however, get trapped in an undesirable local minimum. One such condition can be created if previously optimized intensity distributions are employed in reoptimization (Zhang et al 2004). Stochastic global optimization methods have the advantage of having an ability to avoid getting trapped at local minima. The stochastic algorithms usually employ a random search or the allowance for uphill moves, which not only accept changes that decrease the objective function, but also some changes that increase it (Kirkpatrick et al 1983). Although the stochastic algorithms, such as simulated annealing and genetic algorithms have the advantages of avoiding getting trapped in local minima they are much slower than the gradient methods (Li et al 2003, Zhang et al 2004).

Most of the optimization models are based on the user defined weight factors that reflect the importance of the given organ to defined criteria. The objective function is the sum of all the defined weights of critical structures and the weights of target dose goals. The optimality of an IMRT treatment plan, however, is difficult to define. With clinical IMRT treatment plans there are always trade-offs between dose coverage and normal tissue sparing. Prior to the initial optimization it is practically impossible to know, what is the impact of the user defined DVH constraints to the resulting dose distribution of an individual patient. The anatomy between different patients is rarely same and the constraints and weights employed with the earlier patient with resulting good dose distribution might be totally not valid with the next patient. For example, in the planning of prostate cancer the volume of the rectum or bladder is usually different with each individual patient and the dose volume constraints has to be modified to realize an optimal dose distribution for every patient. It is often unclear how strongly the given constraints and objective parameters affect the resulting plan and the best balance of optimization is not known. Solution to define the optimal weight factors and constraints for different organs or the target volumes is nonexistent and practically the values have to be found by trial and error fashion by repeating a number of optimization processes (Wilkens et al 2007, Zhang et al 2006).

3.4.1 Intensity map optimization of IMRT

In most IMRT optimizations the radiation intensity map of the beam is defined by optimizing each bixel (beam pixel) of the beam. The IMRT optimization modifies the beam intensity maps in each iteration and calculates the dose after each modification. After a successful optimization the intensity or fluence maps have to be converted, in a case of MLC delivery technique, to a series of MLC shapes or movements. This is usually executed by a leaf sequencing algorithm, which is a separate optimization for the allowed and possible MLC shapes. The leaf trajectories have to produce a radiation intensity profile that agree with the desired profile with sufficient precision. The MLC

design of each manufacturer imposes restrictions on the possible aperture shapes and the delivered beam intensities might differ from the actual beam intensities. Due to the separation of intensity optimization and leaf sequencing, a large number of apertures are typically required for recreating the optimized beam intensities. Also a large number of complex field shapes are often needed. This will lead to a loss in efficiency of the delivered MUs and an increase in scattered radiation.

3.4.2 Direct aperture based optimization (DABO)

In DABO the shapes or the movements of the MLC are optimized directly and the optimized treatment plan does not require a separate leaf sequencing algorithm. The optimization only considers aperture shapes that satisfy the constraints imposed by the MLC. Additional delivery considerations can also be included in the optimization, such as the minimum aperture size, minimum number of MUs in each subfield and the maximum number of apertures with one beam. By using DABO the IMRT delivery efficiency is increased since the mechanical limitations of the MLCs are taken into account in the plan optimization. DABO can produce highly efficient treatment deliveries with a significant reduction in both the number of beam segments and the number of MUs (De Gersem et al 2001, Shephard et al 2002). Considerable advantages with DABO over conventional optimization methods have been observed in the dosimetric quality and treatment efficiency (Jones and Williams 2008). With the reduction of number of segments and MUs the treatment times are also decreased with DABO (Jones and Williams 2008). The disadvantage of DABO is the less straightforward optimization because of the complex dependence of the dose on the field shapes, and their weights and consequently the optimization can be computationally demanding (Cotrutz and Xing 2003). There are at least two commercial direct aperture based planning systems available (Ahunbay et al 2007, van Asselen et al 200).

3.4.3 Physical and biological optimization

Most of the IMRT optimization algorithms are based on measurable and well-defined physical dose objectives of such as dose and volume. The physical quantities, like minimum and maximum dose of the PTV and OAR, are easy to be realized and the objectives and limits have clinical relevance. In clinical work the normal tissue complication probabilities are estimated usually by a single dose-volume parameter derived from the DVH of the organ. For example, it is recommended that for the healthy lung tissue 30% of the lungs should receive less than 20 Gy, which can also be written as $V20 < 30\%$ (Marks et al 2010). A maximum dose of the spinal cord can not exceed the dose of 50 Gy (Kirkpatrick et al 2010). Current recommendations and limitations of dose-volume constraints for normal tissues have been derived from numerous clinical studies, where the dosimetric parameters of 3D-planning have been associated with normal tissue complications. In physical optimization the planner defines physical dose constraints for each structure of the treatment plan, either in form of minimum and maximum doses or

as dose-volume constraints. A potential problem with dose-volume constraints is that they are non-convex (Deasy 1997). As a consequence, the optimization may get trapped in local minima. However, it has been shown that this is mainly a theoretical problem, which is of little relevance in practical optimization (Wu et al 2002).

Radiobiological models can be utilized to estimate NTCPs and TCPs associated with a particular treatment plan and to evaluate competing treatment plans. In the so-called biological optimization the objective function is based on mathematically defined radiobiological models. Radiobiological models have been utilized in IMRT optimizations although the studies have mainly been theoretical (Olafsson et al 2005, Peñagarícano et al 2005, Stavrev et al 2003). The use of biological IMRT optimization models has improved normal tissue sparing and target dose coverage when compared to the conventional dose-volume optimizations (Peñagarícano et al 2005, Qi et al 2009, Semenenko et al 2008). Biological IMRT optimization models have not yet, however, been widely adapted to clinical setting. The main reason for this is the uncertainty of the current radiobiological models and the limited knowledge of the tumour control and normal tissue toxicity probabilities (Das et al 2009). One reason for the popularity with the physical, such as dose and dose-volume constraints in the clinical setting might also be the wide clinical experience with the dose-volume limits (QUANTEC, Bentzen et al 2010).

Several radiobiological models have been developed to describe the dose response to heterogeneous dose distributions for tumours and normal tissues. Biological normal tissue toxicity can be modelled with linear-quadratic (LQ) cell survival model (Fowler 1989, Brenner et al 1998), relative seriality NTCP model (Källman et al 1992), parallel architecture NTCP model (Jackson et al 1993, Yorke et al 1993) or Lyman-Kutcher-Burman (LKB) NTCP model (Kutcher et al 1991, Luxton et al 2008, Lyman 1985). The probabilities of tumour control can be modelled with LQ-Poisson TCP model (Källman et al 1992), generalized equivalent uniform dose (gEUD) model (Niemierko 1997), LQ-Poisson model with interpatient heterogeneity (Sanchez-Nieto et al 2001, Webb and Nahum 1993) and an individual TCP model (Zaider and Minerbo 2000). In clinical work the biological models support the clinical decision making. The models can also be used as predictive values although they are simplified and limited by uncertainties in the model parameters.

In the LKB model the NTCP for uniform irradiation is given by

$$\mathrm{NTCP} = \frac{1}{\sqrt{2\pi}} \int_{-\infty}^{t} \mathrm{e}^{-\frac{t^2}{2}} dt \tag{3-1}$$

where

$$t = \frac{D - \mathrm{TD}_{50}(V)}{m\,\mathrm{TD}_{50}(V)} 100 \cdot \tag{3-2}$$

V is the partial volume of critical organ, D the uniform dose to the organ, $\mathrm{TD}_{50}(V)$ the partial organ dose for which the NTCP is 50% and m is a dimensionless parameter which affects the steepness of the dose-response curve. The volume dependency is usually represented by a power-law relationship

$$\mathrm{TD}(V) = \mathrm{TD}(1) / V^{n} \tag{3-3}$$

where TD(V) is the tolerance dose for a given partial volume (V), TD(1) is the tolerance dose for the full volume and n a fitted parameter which represents the volume dependence of organ.

The TCP models assume that the number of potential stem cells is directly proportional to tumour volume (Brenner 1993). The non-Poissonian dose-time dependent TCP model of Zaider and Minerbo (ZM-model) is based on birth and death processes to include cellular repopulation (Zaider and Minerbo 2000). The individual TCP can be calculated with different time intervals between any two consecutive fractions. Based on the ZM-model a TCP formula for fractionated RT has been derived (Stavreva et al 2005). The TCP-model parameters include overall treatment time (T_{n-1}), total initial number of clonogens (N), tumor repopulation rate (λ), time until the kth fraction (T_{k-1}) and cell survival probability after each fraction. Based on LQ-model the cell survival probability after the kth fraction of dose delivery can be expressed as

$$p_s(T_{k-1}) = \exp\left(-\alpha \sum_{i=1}^{k} d_i\right) \exp\left(-\beta \sum_{i=1}^{k} d_i^2 - 2\beta \sum_{i=1}^{k-1} \sum_{j=i+1}^{k} d_i d_j e^{-(T_{j-1} - T_{i-1})/\tau}\right) \tag{3-4}$$

where τ^{-1} is the probability of cell repair per unit time, $T_{j-1} - T_{i-1}$ the time interval between the fractions, α and β are the cell radiosensitivity characteristics, n the number of fractions and d_i and d_j the dose per fraction.

At present, the ZM-model is the most adaptable probability model for tumour control since it can accommodate any fractionation schedule and the model can be can be extended to more sophisticated cell population models (Hillen et al 2010). However, the model can overestimate the TCP if it does not account for less radiosensitive cells (O'Rourke et al 2009). For example the cells in "rest" phase (G0) are less sensitive to radiation than the proliferating cells. This can be accounted for by the use of a model proposed by Dawson and Hillen (2006) in where they have split the tumour cell population into two compartments. This will, however, give a quite complex TCP formula which is not practical in IMRT optimization.

A probability of uncomplicated control (PUC) can be calculated from the TCP and NTCP (Ågren et al 1990). The uncomplicated control is the probability of local tumor

control without normal tissue complications. The basic principle of the PUC is to balance between the radiation benefits and risks in terms of biologic response. The PUC can be calculated by

$$PUC = TCP - P_I + \delta P_I (1 - TCP) \tag{3-5}$$

where P_I is the probability of injury and δ the fraction of patients for whom the local tumor control and radiation-induced injury are statistically independent. The value of δ was set to 0.2 (Ågren et al 1990). P_I can be written as

$$P_I = 1 - \prod_1^i (1 - NTCP_i), \tag{3-6}$$

where i denotes the number of critical normal tissues in the treatment area.

3.5 Dosimetry of IMRT

With 3D-CRT the independent MU checks are possible to calculate manually to limit errors and flaws in implementation and treatment planning. The increased complexity in IMRT makes the MU calculations more demanding for the TPSs and the correct MU settings can not be verified by manual calculation. To verify the dose predictions of IMRT planning systems they have to be compared with measurements. Discrepancies between calculated and measured doses may be due to three different sources: 1) accuracy of the dose calculation algorithm, 2) accuracy of the measurements or 3) errors in beam delivery. The more frequent and the higher the dose gradients in the delivered radiation fluence are the more the potential errors are increased in dose calculation.

3.5.1 Dose calculation algorithms and IMRT

The dose calculation process in modern radiotherapy is usually divided into the prediction of radiation fluence and prediction of the energy deposition within the patient. The treatment machine and the field modulating devices are modelled in the calculated energy fluence. These include blocks, collimator shapes, field penumbra, MLC leaf leakage and T&G effect. In IMRT dose calculation the MLC leaf motions are converted to fluence patterns before the initial dose deposition calculation. The accuracy of these conversion algorithms varies with the complexity of the intensity modulation present in the IMRT field (Mihaylov et al 2006). The calculation of the final dose distribution within the patient is based on the predicted radiation fluence. The complexity of MLC based IMRT dose delivery introduces greater demands for the dose calculation algorithms and for their accuracy.

A practical dose calculation model should be fast and accurate for all beam arrangements. The dose calculation accuracy, especially in the regions of tissue inhomogeneities with electronic disequilibrium, depends strongly on the calculation algorithm and the density

of the medium (Aarup et al 2009, Carrasco 2004, Panettieri 2007). The most challenging for dose calculation algorithms are very small field sizes and heterogeneous conditions. Clinically available dose calculation models can be divided into three categories: 1) Type-a calculation algorithms (for example pencil beam convolution (PBC)) in where the density changes are sampled along the primary rays and changes in lateral transport of electrons are not modelled (Knöös et al 2006). 2) Type-b calculation algorithms (like anisotropic analytic algorithm (AAA) and collapsed cone convolution (CCC)) that are able to treat the lateral electron transport in an approximate way. 3) Monte Carlo (MC) simulations, which are considered as the most accurate dose calculation methods in RT.

Type-a calculation models are fast and simple to use and they are frequently utilized in modern RT treatment planning regardless of the inaccurate calculation in heterogeneous volumes. The PBC algorithm fails to model the dose distribution accurately near and in air cavities, leading to an overestimate of the target coverage (Carrasco et al 2004, Partridge et al 2006, Van Der Voort Van Zyp et al 2010). The calculation inaccuracy increases by decreasing the field size and increasing the volume of the inhomogeneity. In homogeneous water equivalent medium the calculation accuracy is generally good.

The type-b algorithms can model the dose more accurately than the type-a algorithms in the case of electronic disequilibrium (Davidson et al 2008, Dobler et al 2006, Panettieri et al 2007). Nevertheless, the type-b calculation algorithms also include inaccuracies depending on the calculation resolution, density of the medium and simplified modelling of electron contamination and scattering (Aarup et al 2009, Fogliata et al 2007, Lydon 2005, Van Esch et al 2006). For example, a type-b calculation algorithm AAA utilizes MC-derived convolution scatter kernels and models primary photons, scattered extra-focal photons and contaminant electrons separately (Oinam and Singh 2010, Ulmer et al 2005). The photon energy spectrum, mean radial energy and scatter kernels are predefined for water equivalent medium and scaled to the densities of the patient during calculation. Tissue heterogeneities are accounted anisotropically in three dimensions by scaling the photon scatter kernels in 16 directions based on electron density. The final dose distribution is calculated from the photon and electron dose convolutions. Good agreement between the AAA and measurements has been reported for various sites like prostate, parotid, nasopharynx and lung (Bragg et al 2008, Fotina et al 2009, Ottosson et al 2010). The difference between the commercially available MC dose calculation and type-b calculation algorithms has been reported to be small (Fotina et al 2009).

Monte Carlo simulation of absorbed dose distributions is considered to be the most accurate dose calculation approach (Ahnesjö and Aspradakis 1999). In MC simulation the radiation interactions though the treatment head and radiation interactions in the patient are simulated by millions of probability calculations. With the applied MC dose engines the dose has to be calculated with a specified statistical precision. The higher the statistical precision of the simulation the longer is the time for dose computation. To be able to achieve a dose precision with a less than 2% statistical precision the dose computation times will be time consuming (Keall et al 2000, Siebers 2008). The MC

methods have not been fully implemented for routine treatment planning of photon beams mainly due to their long calculation times. Although the efficiency of the MC simulations has been increased by variance reduction techniques and density thresholding the main problem is the statistical accuracy within the limited calculation time (Siebers 2008).

With standard MC codes the simulation of the full radiation transport would take hours. With clinically available Monte Carlo based calculations some variance reduction techniques have been used to speed up the calculation process (Petoukhova et al 2010). Because of the simplifications deviations up to 5% have been observed with small field sizes (24×24 mm^2) and inhomogeneities in treatment field (Petoukhova et al 2010). The increased amount of radiation penetrating the MLCs with IMRT might cause the inaccuracies in MC dose calculations since MLC leaf shape modelling has limitations and thus the interleaf transmissions are not modelled accurately (Ottosson et al 2010).

The modulation of beam intensities by the MLC introduces new uncertainties in the accuracy of dose calculation. The transmission through MLC becomes more pronounced since the leaves are covering the target volumes and a large amount of radiation dose is penetrating the MLC (Zygmanski et al 2007). Also the beam transmission is not uniform over the area of the MLC because of the divergence of the radiation and the interleaf transmission of the MLC (Lorenz et al 2004). Radiation passing through the MLC has also a higher energy than the corresponding open field radiation due to a beam hardening effect and this affects the depth dose properties of the transmitted radiation (Wu et al 2011, Zygmanski et al 2007). Usually the dosimetric properties are taken into account in the TPS by two parameters: 1) dosimetric leaf separation (DLS), which takes into account the increased beam transmission in the rounded leaf ends of the MLC. If the rounded leaf ends are not modelled by the calculation algorithm the calculated doses will be underestimated by as much as 45% for a 0.1 cm wide aperture (Lydon 2005). 2) MLC transmission, the average amount of radiation that will penetrate the MLC. The average MLC transmission increases with the field size, but commercial treatment planning systems use only a single value for it (LoSasso 2008). Radiotherapy dose calculation methods need evidently additional parameters to account for the dosimetric properties of the MLC.

3.5.2 Dose measurements of IMRT

The IMRT fields have to be measured to verify the dose delivered since the manual calculation of the very complex apertures, employed in 3D-CRT, is practically impossible. In IMRT dose verifications the optimized fluences in patient geometry are usually applied to a CT scanned phantom geometry made of water or water equivalent plastic. The dose is recalculated in the phantom geometry and the dosimetric verification is between the measured and calculated phantom dose. Measuring the IMRT dose distributions and the spatial locations of the dose gradients is critical to safe implementation of IMRT (Low et al 2011). The use of IMRT leads to complex dose distributions with steep dose gradients within the target volumes. As a consequence the measurements have their own

challenges due to the absence of charged particle equilibrium, positioning problems of the detector and the effects of detector size.

An optimal dosimeter would have traceability to a primary calibration standard, good stability, linear dose response, high spatial resolution and independent of beam quality or direction (Low et al 2011, Pappas et al 2008). There is also a demand for tissue equivalency and for the independence of response to energy with IMRT measurements because of the increased scatter from the treatment head and MLC and also the increased amount of radiation transmitted through the MLC. However, each dosimeter has a limited spatial resolution and accuracy to verify the measured dose. For example, the spatial resolution of typical ionization chamber is low due to the volume averaging effect in the active chamber volume. The volume averaging effect is associated with small field sizes and is observed within beam penumbra regions which will cause inaccuracies in absolute dose and dose distribution measurements. The IMRT measurement devices can be categorized to point, 2D- and 3D-dosimeters.

Point dosimeters

With point dosimeters the dose can be measured in one point at a time. Consequently the point dosimeters can not be applied in IMRT to verify the 2-D radiation distributions. Point dosimeters include ionization chambers, semiconductor diodes, diamond detectors, thermoluminescent dosimeters (TLD) and metal oxide semiconductor field effect transistors (MOSFET). Ionization chambers are used as a reference dosimeter in RT to define the absolute dose delivered by various external beam devices. To be able to convert the measured signal to absorbed dose in medium the use of ionization chamber requires calibration of the chamber and corrections for recombination and polarity in reference conditions. The reference conditions require an electronic equilibrium in the measured volume. The use of small IMRT apertures usually violates these conditions and the electron fluence distribution in the chamber is altered and volume averaging effect takes place (Bouchard and Seuntjens 2004). If IMRT point dose calculations are compared against the measurements, the measurement point should be set to a position where dose gradients are minimal. The volume effect of the measurement chambers can be reduced by contouring the active volume of the chamber in the TPS and use dose-volume statistics to determine the average dose value (Low et al 2011). The volume averaging method allows the use of larger ionization chamber volumes and thus the positioning error of the chamber can be reduced. If using the volume averaging method the possible limitation of dose calculation resolution of the TPS has to, however, be considered carefully. Silicon diodes have a better spatial resolution than the ionization chambers, but their response to radiation depends also on the spectral composition of the radiation beam (Bucciolini et al 2003, Eklund and Ahnesjö 2010). Since the absorption coefficient of silicon is higher than that of water the dose from low energy photons might be overestimated. Diode detectors have a tendency to lose sensitivity with a function of absorbed dose and have also an angular response (Griessbach et al 2005).

2D-dosimeters

With IMRT treatments the radiation fluence distribution is not uniform within the field and consequently the point dosimeters are not ideal in the dose measurements. 2D-detectors are required to verify the dose distributions of IMRT since they measure the dose in a plane. The most widely utilized 2D-dosimeters are radiographic or recently the radiochromic films. Unlike radiographic film, radiochromic film does not require processing for generating the optical density response to ionizing radiation (Richley et al 2010). The films are self developing and flatbed scanners with transmission mode can read the optical densities of the films. Radiochromic films have a high spatial resolution of at least 0.1 mm, they are near tissue equivalent and have a low energy-dependency (Fuss et al 2007). The films can be inserted in phantoms, which make them practical in IMRT dose verifications. The problem of film measurements is the measurement noise, which is greater than with the other dosimetry techniques used in RT dose measurements. The scanning and analysing of the irradiated films is time consuming and there might be variations in film sensitivity caused by film batch and due to film scanning artefacts (Low et al 2011). The overall measurement uncertainty is about 4% with a single film and when averaging two or more films 1.3% uncertainty is achieved with careful film handling (Richley et al 2010, van Battum et al 2008).

Amorphous silicon based electronic portal imaging devices (EPID) can be used as 2D-detectors. The radiation generates electrons in a copper plate. The electrons then interact with a scintillating material which in turn interacts with a photo-diode on each point on the array. The generated charge is recorded over a 2D-grid. EPIDs were originally designed as imaging devices and as a result they do not inherently measure dose in tissue equivalent media (Nelms et al 2010). EPIDs have a high spatial resolution of about 0.4 mm and typically a large active area of 40 cm × 30 cm. The EPIDs response to radiation is not equivalent to the dose to water measurements since the density of copper deviates from the density of tissue. Consequently the response is more sensitive to MLC transmitted radiation (Vial et al 2008). Nevertheless, the EPID is reproducible and self-consistent, which makes it excellent to quality assurance measurements (Van Esch et al 2004). The application of EPIDs to IMRT is limited to measurements of individual fields. Many corrections must be applied to convert the resulting signal into dose. Also the fluorescent screen leads to an over-response of the detectors to low doses (Low et al 2011).

2D-arrays or matrixes use multiple point detectors to measure dose distribution. Hundreds of point detectors, either ionization chambers or diodes, are aligned usually in one plane and in a simple geometry. Multiple cumulative readings are taken during the IMRT-delivery verification and the results are available instantly after the dose delivery. The detector centre to centre distance of the 2D-arrays is usually between 5 to 10 mm. The spatial resolution is consequently much lower than with the films or EPID dosimeters. However, when the detectors lateral response function is applied the measurement resolution is increased to be appropriate for the IMRT dose verification (Poppe et al 2007). Two-dimensional diode or ionization chamber array detectors have

yielded equivalent dosimetric results when compared to film measurements (Chandraraj et al 2011).

3D-dosimeters

IMRT dose distributions can be measured in 3D with individually fabricated chemical gel dosimeters. Polymer gel dosimeters can be fabricated from radiation sensitive chemicals when they are both the phantom and the dosimeter. The degree of polymerization reaction of the gel is a function of dose. High resolution 3D maps can be achieved by magnetic resonance (MR) scanning, optical-CT scanning, X-ray CT or ultrasound since the polymerization affects the MR relaxivity of water protons and the optical scattering of the gel (Baldock et al 2010). Polymer gels are soft-tissue equivalent with properties that may be modified depending on the application. The gel dosimeters eventually lose the recorded dose distribution with time. Therefore, the dosimeters must be scanned within 2 h of irradiation (Low et al 2011). The fabrication of the gel dosimeters takes considerable time and dose calibration curve has to be generated from the same batch, as for the film dosimeters (Das et al 2008, Low et al 2011). The dose-response of the dosimeters can be dose rate dependent and differences in temperature history after fabrication may compromise the dosimetric accuracy (Baldock et al 2010). The final dose deviation can be reduced to less than 3% relative to the dose maximum, if at least 10 mm away from the surface of the gel container (De Deene et al 2007).

4 FEASIBILITY OF IMRT

IMRT has been used in RT treatments of head and neck (H&N), prostate, breast, cervical and many other cancers (Cozzi et al 2008, Lauve et al 2004, Liu et al 2004, Lohr et al 2009, Zelefsky et al 2002). In this study the feasibility of IMRT was evaluated in H&N cancers with DABO (III) and the method of SIB IMRT based on biologic images was investigated with PCa (IV). The ability of IMRT to deliver uniform dose distribution with a single treatment plan in CSI was evaluated in (I). Finally the dosimetric accuracy of calculation algorithms was analysed with a phantom simulating lung tumours with the very small beam apertures and in heterogeneous patient geometries (II).

4.1 IMRT in various treatment sites

4.1.1 Head-and-neck cancers

The target volumes of head-and-neck cancers are usually very complex and concave. Adequate dose coverage is practically impossible to achieve with 3D-CRT techniques without violating the dose limits of critical normal structures. The concave shapes of the target volumes and the various OARs make the IMRT ideal for treating patients with H&N cancer. An example of a concave target volume of H&N patient is illustrated in Figure 4-1. The greatest benefit from IMRT is the avoidance of critical structures, especially salivary glands. The benefit is seen as reduced incidence and severity of xerostomia (Nutting et al 2011, Pow et al 2006, Saarilahti et al 2006). The ability to reduce spinal cord doses with IMRT has increased the target coverage of the PTVs and consequently fewer compromises are needed with the treatment dose to the target volume. IMRT has also the potential to decrease the doses delivered to pharyngeal constrictor muscles, inner ear structures and oral cavity (Eisbruch et al 2004, Peponi et al 2011, Petsuksiri et al 2011). With the avoidance of critical organs the quality of life of the IMRT treated head-and-neck patients has increased significantly when compared to patients treated with 3D-CRT (Pow et al 2006, Nutting et al 2011).

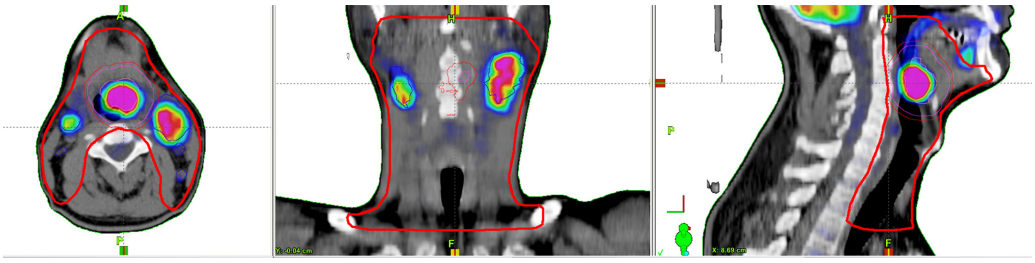

Figure 4-1. CT-images of the concave PTV of a H&N cancer patient highlighted with red colour in transversal, coronal and sagittal planes. The uptake of [^{18}F]fluoro-2-deoxy-glucose (FDG) represents metabolic activity of the tumour imaged with PET (shown with colour distribution).

4.1.2 Prostate cancer

Multiple studies have shown that tumour control is improved with dose escalation in external beam RT of localized PCa (Kuban et al 2008, Kupelian et al 2008, Zelefsky et al 2008a, Zietman et al 2005). Even ultra-high doses over 80 Gy are recommended for more aggressive tumours to increase the tumour control (Eade et al 2007). The dose escalation will, however, result in higher rates of radiation induced late toxicities unless the treatment volume is decreased or the dose distributions are altered to spare more critical organs, especially rectum and bladder (Chism et al 2003, Dearnaley et al 2007).

Although the shapes of the target volumes of the local PCa treatments are relatively simple, as shown in Figure 4-2, the close proximity of critical organs makes the high dose treatments challenging. With IMRT the doses to organs at risk (rectum, bladder, hip joints, small bowel, penile bulb) can be decreased and consequently the toxicity of the given RT treatment is decreased. Compared with 3D-CRT, IMRT has significantly reduced acute and late toxicities (Metwaly et al 2008, Sharma et al 2011, Zelefsky et al 2008b). In addition the irradiation of hip joints can be avoided with IMRT as 3D-CRT treatments have been associated with a 76% increased risk of hip fracture (Elliott et al 2011).

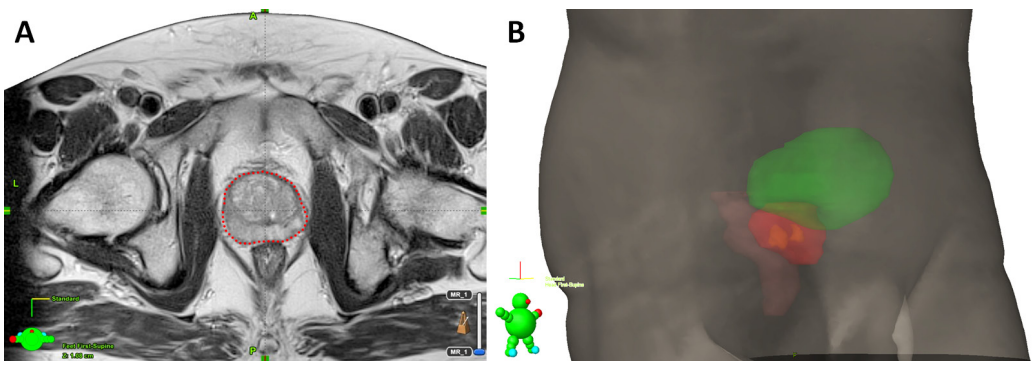

Figure 4-2. In RT of PCa the shape of the target volume (red) is circular as visualized in a transverse MR image (A). The close proximity of OARs, like rectum and bladder, contoured with brown and green colour in (B), respectively, makes it challenging to deliver high doses of radiation to the prostate without normal tissue toxicity.

4.1.3 Craniospinal irradiation (CSI)

CSI is often utilized in the treatments of primitive neuroectodermal tumours (PNET) of the central nervous system. Typical target volume of the CSI is shown in Figure 4-3.

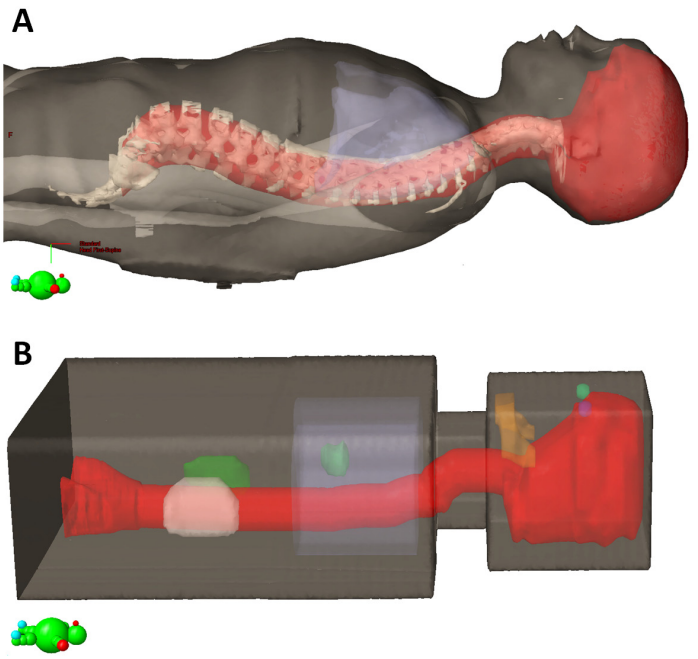

Figure 4-3. Long target volume (red) of the CSI (A) and a phantom simulating the patient geometry with a possibility to insert dosimetric films inside (B).

CSI is technically very challenging to execute because the treated volume is larger than the largest possible field sizes with a standard linear accelerator. The use of multiple isocentres in the treatment delivery will introduce large dose gradients and overlapping areas in the field junctions. This will easily produce dose inhomogeneities and unwanted hotspots in spinal cord. Different methods have been developed to increase the PTV coverage and the safety of the treatments (Koshy et al 2004, Michalski et al 2002, Parker and Freeman 2006, South et al 2008, Tenhunen et al 1994, Verellen et al 1996, Wilkinson et al 2007, Yom et al 2007). However, none of the introduced techniques has been able to overcome the problem of high dose gradients when the different isocentres are used. Consequently, the 3D-CRT treatments are highly dependent on the mechanical accuracy of the treatment delivery and patient positioning.

4.1.4 Pulmonary tumours

Non small cell lung cancers (NSCLC) have been treated with IMRT with the aim of reducing doses to the lungs, the major dose limiting organ during radiotherapy of thoracic cancers. The IMRT planning improves target coverage and reduces the high-dose volume of lung (Christian et al 2007, Liu et al 2004, Murshed et al 2004). When IMRT has been used with 4D-imaging techniques the overall survival has been higher than with the 3D-CRT treatment delivery (Liao et al 2010). IMRT and VMAT have also been utilized in treatments of SLRT and proposed as the best practical approach for the delivery of SLRT (McGrath et al 2010, Verbakel et al 2009b, Videtic et al 2010). In

SLRT treatments the maximum tumour size has to be smaller than 6 cm (De Ruysscher et al 2010). The small field sizes and the low density of lung creates challenges to the dose calculation algorithms accuracy, even with conventional 3D-CRT beam delivery (Dobler et al 2006, Jones and Das 2005, Panettieri et al 2007, Sikora et al 2009). An example of the small target volume surrounded by lung is shown in Figure 4-4.

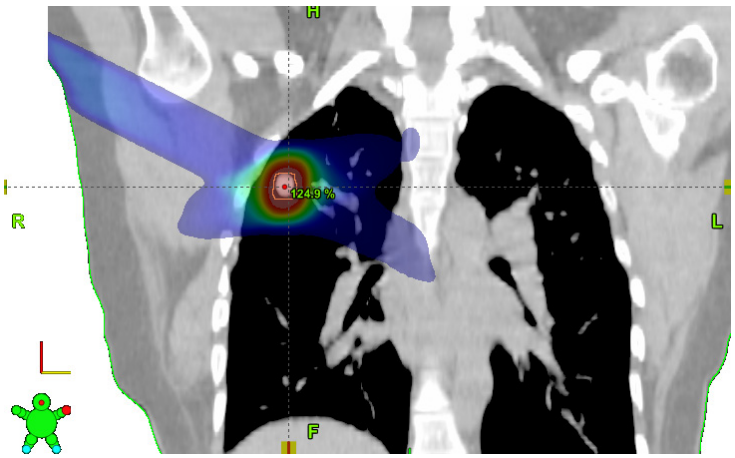

Figure 4-4. A small target volume of SLRT imaged in a coronal plane of CT image with planned dose distributions in colour isodoses.

The use of IMRT decreases the effective aperture sizes when compared to conventional 3D-CRT. Thus the rebuild-up and rebuild-down effects are potentially increased in the lung tumour interfaces. The dose calculation algorithms are still based on approximations in calculating the absorbed dose in the patient. The accuracy of these approximations determines how well the radiation dose distribution is modelled in the heterogenous patient that is how well the model is able to account the energy transfer from primary photons, scattered electrons and photons within the radiation field. Therefore, IMRT could be suboptimal in lung treatments because of the possible inaccuracy of dose calculation algorithms to accurately model the dose in heterogeneous media.

4.2 IMRT with multiple isocentres

With very large treatment volumes the mechanical limitations of the linear accelerators prevent the RT treatments to be delivered with a single isocentre. Typically with CSI the beam edges from different isocentres are matched geometrically. Because of the beam divergence the matching can be realized in one point only. Alternatively, rotations of treatment couch and collimator can be utilized to match the beam is one plane. With the traditional 3D-CRT beam matching techniques the dose gradients are very high in the beam junction areas. This will make the treatments very vulnerable for geometrical uncertainties present in the treatment delivery (Carrie et al 1999).

sfIMRT can be employed to accomplish uniform dose distribution in the junctions with low dose gradients. The method eliminates the field matching problems associated with the conventional beam matching. Generally the split field technique is used in large treatment volumes where the physical limitations of the MLCs restrict the dose delivery with one sliding window sequence. With a plan having two or more isocentres the fields can be adjusted to overlap with fixed collimator jaws to ensure adequate overlapping region between the adjacent fields. With dynamic feathering the subfields overlap each other by a small amount and the sum of the intensities of the subfields remains the same as for the original field. At least a 3-cm overlap is needed to avoid sharp dose gradients (Malhotra et al 2005). The overlapping subfields create a large feathering area which reduces the sensitivity to displacement errors at the field junction region due to uncertainties in setup and organ motion. DMLC technique can produce a uniform junction easily by using multiple control points but in SMLC the treatment field needs more than 20 segments to achieve a uniform dose distribution (Wu et al 2000b).

4.3 Simultaneous integrated boost (SIB) treatments

RT often involves two or more phases, when the irradiation of microscopic disease is followed by a sequential dose escalation with another treatment plan to a smaller target volume containing only gross tumour volume (GTV). In simultaneous integrated boost (SIB) two or more target volumes is designed to receive different prescription doses with the same treatment plan. IMRT has the potential to create different dose areas to various target volumes within a single treatment fraction thus allowing dose escalation to the defined volumes of interest.

There is evidence that shortening overall treatment time in RT of head and neck squamouscell carcinoma improves locoregional control because of better control of the rapidly proliferating tumour clonogens (Horiot et al 1992, Overgaard et al 2010). The ability of IMRT using the SIB technique has established new means to apply accelerated fractionation with little increase in normal tissue toxicity. The SIB-IMRT can be used to deliver higher radiation doses to pre-defined high risk areas such as GTV compared to surrounding clinical target volume (CTV) which receives a standard dose. SIB-IMRT appears to be an effective strategy in the treatments of H&N cancers and SIB-IMRT treatments have been reported to reduce the toxicity without compromising the treatment outcome (Al-Mamgani et al 2009, Orlandi et al 2010).

The SIB-IMRT technique is feasible in many treatment areas including H&N, prostate, oesophagus, gynaecological and breast cancer. The biological effectiveness, the better sparing of critical structures and the reduced treatment duration by the SIB-IMRT has been confirmed in multiple studies (Chen et al 2005, Cho et al 2010, Guerrero et al 2005, Li et al 2005, McDonald et al 2010). However, in one study the results have been contrary and sequentially delivered boost technique resulted in a better treatment plans with less dose to the parotid glands (Lamers-Kuijper et al 2011).

4.4 Dose painting and IMRT

Traditionally, the basic principle of RT has been to deliver a uniform dose distribution to the defined target volume. However, the uniform dose distribution does not give optimal tumour control probability when the tumour cells have variable radiosensitivity within the target volume (Mackay and Hendry 1999, South et al 2009, Søvik et al 2007b, Tomé and Fowler 2002). The routine clinical treatment planning does not take into account the various radiation sensitivities in the treated volumes.

The hypothesis of dose painting is to increase the TCP by delivering higher radiation doses to the areas of the patient having the greatest probability of locoregional recurrences (Ling et al 2000). One reason for the local recurrence might be due to a tumor-specific microenvironment, for example hypoxia. Several imaging techniques of MRI and PET are available to image molecular and biological properties of the tumour like tumour metabolism, tumour burden, low oxygen areas (hypoxic volumes) and tumour perfusion that are relevant for the outcome of radiation treatment (Brændengen et al 2011, Price et al 2006, Troost et al 2010). Consequently the accuracy of the utilized imaging methods to define the most radioresistant areas is crucial in the success of dose painting.

So far the dose escalation strategies by dose painting have mainly been theoretical and retrospective. The clinical data is sparse from the normal tissue toxicities or possible recurrences in the treatment area. However, many modelling studies of the potential to increase TCPs have been performed to estimate the efficiency of different dose escalation strategies (Malinen 2006, Petit 2009, Popple 2002, Søvik 2007a, Søvik 2007b, Thorwarth 2007, Tomé 2000). The focus on the dose painting studies has been mainly on the TCPs while the possible increase in NTCPs with high doses have not been modelled.

Different dose escalation strategies have been proposed. One is to selectively boost the dose to the radioresistant volumes while keeping the integral target dose constant (Petit 2009, Sovik 2007a). The other approaches are to give additional boost dose to resistant volume (Lin 2008, Popple 2002, Tomé 2000) or the dose escalation strategy can be planned with respect to target coverage at constant normal tissue toxicity (Thorwarth 2007). Whatever the strategy is being applied, IMRT has provided the ability to modify the delivered dose distribution by dose painting. The dose escalation to the resistant cells can be realized by dose painting by numbers (DPBN) or by quantitating the biological parameters into few discrete levels, dose painting by contours (DPBC).

4.4.1 Dose painting by numbers

In DPBN the dose prescription in each voxel is based on the voxel intensity of the image of radioresistance (Bentzen 2005). Dose-painting IMRT optimizations for spatially inhomogeneous radiosensitivity have been developed that have been speculated to lead to increased treatment effectiveness (Chen et al 2007, Kim and Tomé, 2010). DPBN lacks the conventional margin approach for geometric uncertainties. However, this can

be corrected in the software by using geometric uncertainties in treatment planning optimization (Witte et al 2011). The resolution of the functional image and beamlet dimensions of the delivery technique limit also the spatial scale to which the radiation dose can be painted to (Bowen et al 2009).

4.4.2 Dose painting by contours

In DPBC the potentially radioresistant target volumes are contoured in the TPS. These volumes can then be utilized in IMRT optimization to target higher discrete dose levels of radiation. The advantage in DPBC is that the segmented volumes can be applied in standard commercial TPSs (Meijer et al 2011). With DPBC the possible uncertainty in the treatment delivery can be accounted for by adding margins around the biologically defined treatment volumes. The more threshold levels of the biological images used in the delineation, the closer the DPBC is with DPBN. The number of levels used in treatment planning is dependent on the radioresistant distribution within the target but increasing the number of levels beyond four yields only little additional benefit (South 2009, Søvik 2007a). From a clinical perspective it can not be determined which approach, DPBC or DPBN, is favourable for the patients.

Chao et al (2001) were the first to demonstrate the feasibility of biological target volumes in IMRT treatment planning with a H&N patient by escalating the dose in BTV without compromising normal tissue sparing. MRI, magnetic resonance spectroscopy (MRS) and choline PET have been used in the treatments of PCa to image potentially more radioresistant intraprostatic lesions (IPL) and DPBC has been used with IMRT (Fonteyne et al 2008, Niyazi et al 2010, van Lin et al 2006).

5 DRAWBACKS OF IMRT

With IMRT the dose coverage of the PTV can be increased, the dose to the OARs can be decreased and SIB treatments can be designed to more radioresistant partial volumes. Unfortunately there are also some limitations with IMRT.

IMRT beam delivery is divided into small beamlets to produce the required non-uniform intensity map. This introduces complexity into IMRT treatment planning and an increased number of MUs is required to deliver the prescribed dose to the patient. The delivery of the modulated fields requires 2 to 5 times more MUs than 3D-CRT (Craft et al 2007). The increase in MUs is associated also with increased treatment times. The beam intensity fluence complexity is associated with decreased dosimetric accuracy, the dose from small apertures is more demanding to calculation algorithms and a greater proportion of dose delivery is coming from leakage radiation of the MLCs, scattered radiation of collimators and head leakage. Consequently, precise dose calculation with IMRT requires an algorithm to model the primary and scattered dose in the heterogeneous patient accurately.

5.1 Aperture size in beam modulation

IMRT is usually delivered by multiple static MLC apertures or by sliding window MLC. The more complex the treated volume is (concave PTV, multiple critical organs, overlapping of OAR and PTV) the smaller are usually the beam apertures. The disadvantage of the small apertures means that the delivered dose is highly sensitive to MLC positional errors and the dosimetric settings of the MLC. For example, with Varian MLC an offset of radiation field is needed to compensate for the increased transmission of the rounded leaf ends. In addition the offset varies as a function of distance from the collimator central axis due to the MLC geometry (Vial et al 2006). An error of 1 mm with a sliding window aperture of 1 cm can lead to an error in dose over 10% (LoSasso et al 1998). The inaccuracies caused by small apertures have been recognized and attempts have been made to decrease the effect of the MLC calibration errors by rejecting treatment plans with very small leaf openings (Zygmanski and Kung 2001).

When the effective field size is decreased the total dose delivered through the closed leaves is increased. The accurate calculation of the leaf transmission is though critical. However, the transmission of the MLC have spatial dependence, which consists of variations due to interleaf leakage and the T&G effect, MLC scatter, leaf mount design and beam divergence. Incorrect settings in the TPS can produce large dose delivery errors, particularly in high precision SBRT treatments (Lee et al 2007). For example Eclipse® TPS uses a simplified model of MLC transmission with only one user defined value. The inaccurate determination of MLC transmissions and DLS can lead to inaccuracies in IMRT beam delivery.

5.2 IMRT in heterogeneous volumes

IMRT treatments employ small beamlets, which in general do not provide electronic equilibrium. With homogeneous water equivalent medium this should not cause inaccuracies in dose calculation if the leaf parameters are optimized. However, behind the low density areas like lung tissue, the effects of dose rebuild-up and rebuild-down will be steeper as the field size is decreased (Behrens 2006). The changes in electron transport are the greatest at the tissue interfaces and underdosing will occur adjacent to low-density inhomogeneities. The magnitude depends primarily on the volume of the inhomogeneity, but also on field size, depth, and beam energy (Ahnesjö and Aspradakis 1999, Hunt et al 1997).

The heterogeneity corrections of type-a calculation algorithms are not able to model the lateral electron transport accurately. This can lead to an underdosage of the PTV. Type-a algorithms tend to overestimate the calculated dose inside the low heterogeneity and the effect is more pronounced for the small fields and high energies (Engelsman et al 2001, Fogliata et al 2007). For accurate dosimetry of small fields the correction-based calculation algorithms should be avoided near large heterogeneities, since differences between the calculation algorithms and the delivered dose can be large (Carrasco et al 2004). With the type-b algorithms the results have been more contradictory and the accuracy depends upon beam energy, field size and density investigated (Fogliata et al 2007).

Lung tumours are typically surrounded by very low and heterogeneous electron densities. The effect of narrow IMRT beams on the tumour-lung interface has not been studied in the perspective of peripheral dose coverage of the tumours. In (II) the calculation accuracy of PBC and AAA was investigated with simulated lung tumours with diameters of Ø1.5 cm and Ø4.0 cm with narrow IMRT fields.

5.3 Increased beam delivery time

With conventional fractionation size (1.8 - 2 Gy / fraction) the treatment times are in the range of 2–10 min with 3D-CRT (Ling et al 2010). However, with IMRT the increased number of MUs leads also to an increased delivery times and the decreased effective dose-rate can have potential influence on radiotherapy response. Protraction of RT dose has been reported to decrease biologic effect and delivery times in the range of 15-45 min may significantly decrease cell killing (Fowler et al 2004, Wang et al 2003a). The protraction is probably clinically insignificant for fast growing tumours with a high α/β ratio of about 10 Gy (Kupelian et al 2008) but the effect of radiation protraction is more pronounced with slowly growing tumours with a low α/β value and short repair halftime (Joiner et al 2010). For example, a fraction prolongation of 30 minutes can result in reduction of effective dose of 3.8% and 7.3% for prostate (α/β = 8.7 Gy) and glioblastoma (α/β = 0.6 Gy) tumour cell lines, respectively (Joiner et al 2010). For hypofractionated IMRT the effect can be even more significant (Kupelian et al 2008). For this reason, it has been recommended to minimize dose-fraction delivery time by

keeping the number of beams low, irradiating with a high dose rate and with low number of segments (Kuperman et al 2008, Joiner et al 2010).

5.4 Second cancer risk

The risk of developing a second primary cancer after RT is a well-recognized side effect and represents a major problem for children and long term survivors (Brenner et al 2000, Maule et al 2007, Nyandoto et al 1998, Rubino et al 2003, Xu et al 2008). The possibility of developing second cancer depends on the irradiated volume, dose-rate and dose distribution (Tubiana 2009, Xu et al 2008). The higher is the irradiated volume and dose, the higher is the risk for the second cancers to develop. Although the risk of developing a second cancer from RT has generally been reported to be small (about 2%) the incidence could be as high as 20% with long term survivals (Brenner et al 2000, Nguyen et al 2008, Tubiana 2009, Xu et al 2008). The risks have to be considered when making the treatment decisions.

Second cancer incidents have been found within or next to the irradiated fields (Nyandoto et al 1998) or they can arise outside the main field within low dose areas (Xu et al 2008). It has been reported that the majority of second tumours are observed in the volume receiving less than 6 Gy (Dörr and Hermann 2002) and recently it has been suggested to reduce the volume of tissue receiving total doses above 3.5 Gy (Tubiana 2010)

In IMRT the MUs are increased when compared to 3D-CRT. This will increase collimator scatter and head leakage, which are the dominant sources of the secondary dose (65%) for IMRT (Ruben et al 2011). The collimator scatter and head leakage from 6 MV IMRT fields is reported to be five and three times larger than from 3D-CRT, respectively (Ruben et al 2011). The internal patient scatter is on the contrary about 10% higher from 3D-CRT than from IMRT (Ruben et al 2011). The leakage radiation could be decreased by delivering the IMRT more efficiently by lowering the amount of MUs needed to deliver the prescription dose, for example by using direct aperture base optimization and/or flattening filter free linear accelerators (Kry et al 2007, Vassiliev et al 2006).

The use of IMRT has increased the beam directions to make the target dose more conformal and to avoid critical structures. As a result the volume of small radiation dose is increased in the normal structures. One of the concerns is then the increased volume of low dose radiation with IMRT and VMAT since IMRT techniques are increasing the irradiated body volumes at 5 Gy or less (Arbea et al 2010). It has been estimated that the incidence of secondary malignancies could increase from 1% to 1.75% for patients surviving 10 years with IMRT compared with 3D-CRT technique (Hall and Wuu 2003). Verellen and Vanhavere (1999) calculated that the risk of second cancer increases by a factor of 8 when the MUs of IMRT where 6 times higher than with the 3D-CRT. The risk for second cancer induction has a high degree of uncertainty. The safest way to limit the risks of second malignancy would irradiate with low photon energies (< 8 MV) with good treatment efficiency (i.e. with low number of MUs) and limit the amount of volume irradiated.

6 MATERIALS AND METHODS

Three different MLCs from the same manufacturer (Varian Medical Systems) were utilized in this study with IMRT delivery. Those were 80-leaf Varian Mark II (III), 120-leaf Millennium (I, IV) and 120-leaf high-definition MLC (HD-MLC) (II).

6.1 IMRT in CSI

In (I) we developed a split field IMRT (sfIMRT) technique that can be applied in the treatment of CSI to reduce treatment related inaccuracies and to increase the dose coverage of the large PTV. The retrospective study with five patients was performed to explore the feasibility of IMRT in CSI. The sfIMRT plans were compared to actually treated 3D-CRT treatment plans and the target dose coverage and homogeneity were evaluated. Tolerance range (TR) was utilized to evaluate the dose homogeneities of PTV and spinal cord (Aaltonen et al 1997). The TR was calculated by

$$\mathrm{TR} = \frac{\text{Standard deviation of the dose to target volume (Gy)}}{\text{Average dose to target volume (Gy)}}. \qquad (6\text{-}1)$$

The sfIMRT technique had the same field arrangement than the 3D-CRT technique, but with fixed field sizes that had at least 4 cm overlaps at the junctions of the fields. The effect of treatment related inaccuracies were simulated with a 3 mm longitudinal shift and the resulting dose distributions in the junction areas were compared between the different techniques.

The accuracy of the dose delivery by the new sfIMRT technique was verified by the radiochromic film (Gafchromic EBT; ISP, Wayne, NJ) measurements in a homogeneous phantom made of PMMA (Fig. 4-3B). Films were placed in the junction areas and the accuracy of dose and dose distributions of the IMRT delivery were measured.

6.2 IMRT in stereotactic lung radiotherapy

IMRT and VMAT have been proposed as the best techniques in the dose delivery of SLRT. However, the dosimetric accuracy of IMRT has not been studied with small apertures in heterogeneous volumes. The accuracy of dynamic IMRT treatment deliveries and the effect of small apertures on the peripheral doses of the tumours were studied with challenging beam arrangements and treatment geometries (II).

The effect of lung heterogeneities on tumour central and peripheral doses was studied with energy of 6 MV. Beams were modulated with HD-MLC with a total of 60 leaf pairs with central leaves of width 2.5 mm and the peripheral leaves 5 mm in the isocentre. The dosimetric accuracy of intensity-modulated techniques in SLRT treatments was studied

by phantom measurements. The measurement set-up and the phantom employed in the measurements are shown in Figure 6-1. Two heterogeneous phantoms were designed and reconstructed from polymethyl methacrylate (PMMA), polycarbonate and cork. The heterogeneous phantoms mimicked the lung patient geometry with two different target volumes with a diameter of Ø1.5 cm and Ø4.0 cm surrounded by cork simulating lung. The density of the cork was on average -550 HU which is close to the density of lung in deep expiration phase.

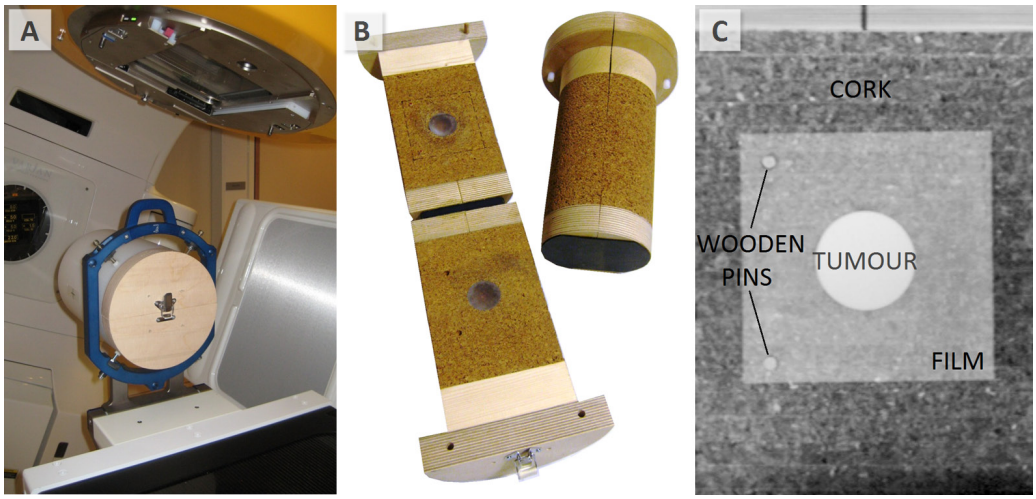

Figure 6-1. Measurement set-up used in (II). PMMA cylinder was attached to a stereotactic frame (A) and the cork cylinders (B) were inserted inside. The patient geometry was simulated with a phantom where the mimicked tumour was located inside lung equivalent material (B). The phantom and film measurements were used to verify the calculated dose distributions of the tumour (C).

The rebuild-up and rebuild-down effects were studied with sliding window apertures (SWA) of 2, 4, 6, 10 and 15 mm and with a 3D-CRT plan, an IMRT treatment plan and two RapidArc plans. The first RapidArc plan (RA1) had dose optimization constraints only for tumour dose coverage and uniformity while the second RapidArc plan (RA2) optimization included also organs at risks specified in the phantom volume. The dose calculations were performed with PBC with modified Batho power law and with AAA with the smallest calculation grid sizes available (1.25 mm and 1.0 mm, respectively). To be able to deliver a prescription dose of 1 Gy to the centre of the tumour, the total number of MUs with various aperture sizes and modulation techniques for small tumour size were 1269, 828, 630, 459, 360, 144, 234, 214 and 247 MU with 2, 4, 6, 10 and 15 mm SWA and with 3D-CRT, IMRT, RA1 and RA2, respectively. For the larger tumour the corresponding MUs were 1809, 1206, 918, 648, 486, 126, 288, 152 and 229, respectively. Measurements were performed both with a micro ionization chamber and with EBT2 (Gafchromic) films. The film measurements were repeated three times to reduce the variability of an individual film.

6.3 Direct aperture based optimization

In (III) a DABO was presented to study the feasibility of direct optimization with five head-and-neck (H&N) cancer patients. The theoretical basis of the investigated DABO has been described earlier (Kolmonen 2002, Kolmonen et al 1998, Tervo et al 2000, Tervo et al 2003). In brief, within the evaluated DABO the objective function is a function of left and right leaf positions and aperture weight. The MLC constraints in the optimization were the inhibition of leaf collision, maximum leaf overtravel of 16 cm, maximum leaf span of 14.5 cm and the avoidance of aperture shapes with multiple openings. A local optimization algorithm of a quasi-Newton method (L-BFGS-B) is used to find the global minimum of the implemented objective function (Kolmonen 2002). When a local optimization algorithm was applied, a method to determine the initial set of aperture shapes was required. For each beam angle, preliminary shapes of the apertures are generated using the BEV of the target volumes and the OARs. During the optimization the feasible solution for the MLC leaf positions and the irradiation times of the subfields is calculated. The studied DABO formalism is based on the use of pencil beam model for the dose calculation. The intensity distributions generated by the MLC are modified with the help of Heaviside function *H*. The dose model for one leaf pair can be modelled as

$$D(x) = \int_0^w h(x,u)H(u-a)H(b-u)du\delta t\,, \tag{6-2}$$

where *x* is a point in a patient, *D(x)* the dose in the point *x*, *w* the width of the treatment field, δt radiation beam-on time and *h(x,u)* the dose deposition kernel. *H(u-a)* and *H(b-u)* are the modified Heaviside functions for the left and right leaves, respectively. Superposition of all leaf-pairs is used to calculate the total dose.

The dose distribution is calculated using the optimized aperture shapes and weights after the optimization. To be able to calculate the dose in the TPS (Cadplan®, Varian Medical Systems, Palo Alto, CA) the optimized apertures were converted to corresponding radiation field fluences from which the dose distributions were calculated. The MUs for each treatment field was calculated based on the dose distribution and dose normalization of the treatment plan. Before the initial direct optimization the directions and the number of static treatment fields were determined. The dose limits for the PTVs and OARs were defined. The maximum number of apertures for each field and the minimum amount of MUs for each aperture were selected. The limits were set to maximum of 9 apertures with one field and minimum 3 MU with one aperture, respectively.

Five H&N cancer patients were retrospectively optimized with DABO and the treatment plans were compared to treatment plans optimized with conventional fluence based optimizations (Cadplan®, Helios®, LMC-version 6.3.5). DABO was realized with SMLC (Mark II MLC) and the conventional IMRT optimizations were realized with both SMLC and DMLC. All the IMRT treatment plans were compared to actually treated

3D-CRT treatment plans. The PTV coverage was estimated with D95 (the minimum dose covering 95% of the PTV) and the dose uniformity was estimated from the standard deviation (SD) of the doses within the PTV.

6.4 Biological treatment plan optimization

The ability of IMRT to cover the whole prostate gland and to deliver simultaneously high doses to small intraprostatic volumes was investigated in (IV). IPLs of 12 patients were imaged with [^{11}C]acetate (ACE) PET/CT. The contoured IPLs were applied to guide SIBIMRT in DPBC to escalate doses up to 90 Gy.

Six different IMRT treatment plans using Varian Millennium MLCs were generated for every patient: a standard IMRT (sIMRT) treatment plan with a prescription dose of 77.9 Gy in 41 fractions to the PTV and five SIBIMRT treatment plans with a dose of 72.2 Gy to the PTV and 77.9 Gy, 81 Gy, 84 Gy, 87 Gy and 90 Gy to the biologically defined target volumes with 41 daily fractions, respectively.

The voxel doses were derived from CT-based TPS (Eclipse®, Varian Medical Systems). The influence of the fraction dose on the cell survival was applied by converting them to 2 Gy equivalent doses based on LQ-cell survival model. Rectal and bladder NTCPs from different IMRT treatment plans were calculated using the LKB model (Kutcher et al 1991, Lyman 1985). The ZM-model was used with the modifications of Stavreva et al (2005) in the calculations of the probabilities of tumour control. The dose per fraction to the biologically defined target volumes (BTV) were calculated with the concept of equivalent uniform dose (EUD) based on the DVH data (Niemierko 1997). The PUCs were calculated for the various treatment plans to derive the optimal radiation dose to biologically guided IMRT PCa treatments.

The patient characteristics in studies (I-IV) are summarized in Table 6-1.

Table 6-1. Patient characteristics in studies (I-IV).

Study	Region	Number of Patients	Irradiation technique	IMRT optimization
I	Craniospinal	5	3D-CRT / sfIMRT	Physical fluence based
II	Lung	2*	3D-CRT / sIMRT / RapidArc	Physical fluence based
III	H&N	5	3D-CRT / SMLC / DMLC	Physical direct aperture
IV	Prostate	12	sIMRT / SIBIMRT	Biological fluence based

* Phantom simulating patient

7 RESULTS

7.1 Feasibility of IMRT

In (I) the feasibility of IMRT in CSI was studied with five patients. The use of dynamic MLC effectively allowed automated intrafractional feathering in a single treatment plan. The split field technique was able to create a homogenous dose distribution to the whole PTV. The sfIMRT improved the target volume coverage and homogeneity. The average volume covered by 95% of the dose prescription was 96.6% with sfIMRT compared to 77.9% for 3D-CRT. The resulting dose gradients in the junction areas were low and the proposed technique was less sensitive to patient motion and mechanical inaccuracies in the treatment. Introduced inaccuracy of 3 mm created a dose error of ± 4% in the spinal-spinal junction. The corresponding error with 3D-CRT technique was ± 37% in the spinal cord.

A TR of 0.06 with sfIMRT versus 0.18 with 3D-CRT (p-value <0.006) was obtained for the spinal cord dose, where a lower TR value indicates greater dose homogeneity. For the PTV the corresponding dose homogeneity values were 0.12 and 0.16 (p <0.03), respectively. Doses to the OARs were comparable between the two techniques. The downsides of the sfIMRT were a doubling of MUs (on average from 611 MU to 1170 MU), an increase in treatment time by approximately 3 minutes (from 13 min to 16 min), and an 8% increase in maximum dose to non-target structures.

The ability of IMRT to cover the whole prostate gland and to deliver simultaneously high doses to small intraprostatic volumes was investigated in (IV). With every patient at least one IPL was detected with ACE PET/CT and 10 patients (83%) had more than one IPL. The uptake of the tracer superimposed on fused CT-images is shown in Figure 7-1.

In Figure 7-1 the dose distributions of a SIB_{78Gy} is shown to boost two separate IPLs. SIBIMRT technique was successfully employed to boost the BTV areas and the introduced biological optimization did not increase the treatment complexity of the plan considerably, when measured by the amount of MUs needed to deliver the prescription dose. The number of MUs for the sIMRT treatment plan to deliver a dose of 1 Gy to the target was on average 281 MU and for the most demanding treatment plan of SIB_{90Gy} the respective value was 297 MU.

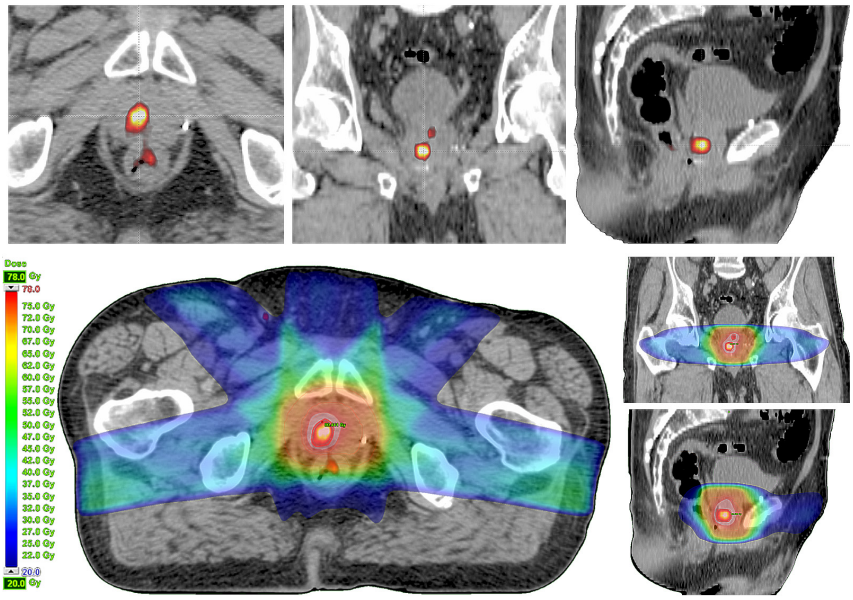

Figure 7-1. The distribution of the [^{11}C]acetate in the prostate in transverse, coronal and sagittal plane imaged by PET/CT. The dose distributions of SIB_{78Gy} are shown below to boost the corresponding IPLs.

7.2 Dosimetric aspects of IMRT

The accuracy of the dose delivery by the new sfIMRT technique in CSI was verified by film measurements in a homogeneous phantom (I). Generally the measured dose distributions were within ± 3% from the calculated values. Sharp edge of the phantom's "neck" (Fig. 4-3B) combined with probably a small geographical error in dose delivery (approximately 1.5 mm) increased the maximum deviation between the calculation and the measurement in the junction area to 7%. Target volumes of the CSI are not in the vicinity of large air or low density areas and thus a phantom with a single density value was employed in the simulated patient measurements. That might be one of the reasons why the measured dose distributions of the IMRT delivery correlated well with the calculated ones. Also the treatment fields were not highly modulated with sharp radiation intensities and the irradiation was delivered with an effective field size close to fields sizes used in conventional treatment delivery.

The effect of lung heterogeneities on tumour central and peripheral doses irradiated with IMRT was studied in (II). The differences between calculated and measured doses were greater with the smaller than with the larger tumour with both the PBC and AAA. With AAA the largest deviation (8%) between the measured and calculated tumour central doses was observed with the smallest SWAs in the smaller tumour. Measurements of the RapidArc treatment plans deviated on average 2.7% (SD 1.9%) from the 3D-CRT plans, while with IMRT treatment plans the difference was on average

0.6% (SD 1.1%). The increased modulation in the RA2 treatment plan decreased the calculation accuracy as the calculation underestimated the central dose of the smaller tumour by 4%.

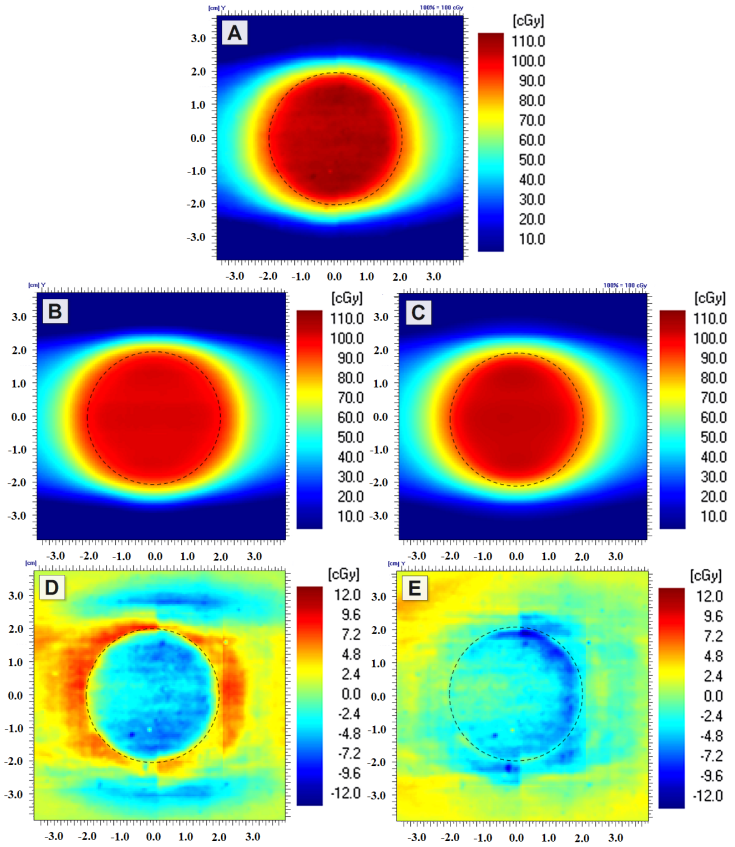

Figure 7-2. The measured dose distribution of the IMRT treatment plan of the Ø4.0 cm tumour (A). The measured doses were subtracted from the calculated dose distributions of PBC (B) and AAA (C) (D and E), respectively. The border line of the tumour is visualized with a dashed line.

Peripheral doses of the tumours were not modelled accurately by the PBC calculation algorithm. This is illustrated in Figure 7-2 where the dose distributions of the film measurements were subtracted from the calculated dose distributions of PBC. PBC overestimated the peripheral doses. The largest difference was 8.1 mm with 95% isodose line when compared to measured values while the average difference was 3.8 mm (SD 1.7 mm) with isodose lines of 80-95%. AAA did not model the dose correctly with the modulated fields near the tissue interfaces (Figure 7-2). AAA underestimated the peripheral doses of the tumours with an average error of 1.1 mm (SD 0.6 mm) with the isodose lines of 80-95%.

Another example of the dose difference between AAA calculation and film measurement of a single field SWA of 4 mm is illustrated in Figure 7-3.

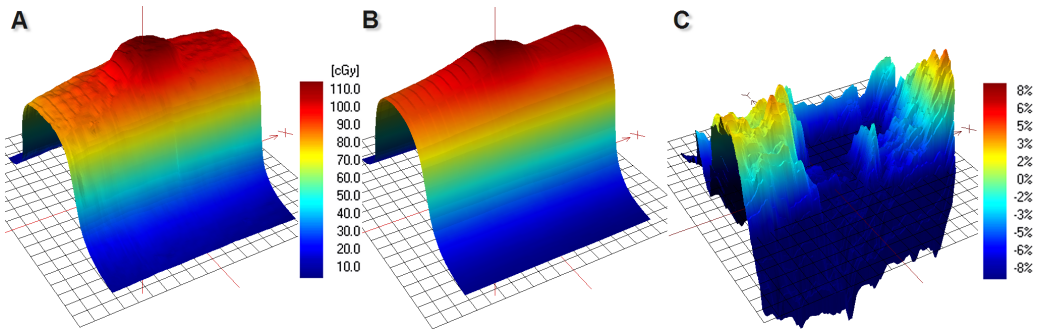

Figure 7-3. Measured (A), calculated (B) and the difference between the two (C) irradiated with a direct anterior 4 mm SWA beam to a Ø1.5 cm target surrounded by lung equivalent material. The calculation algorithm was AAA.

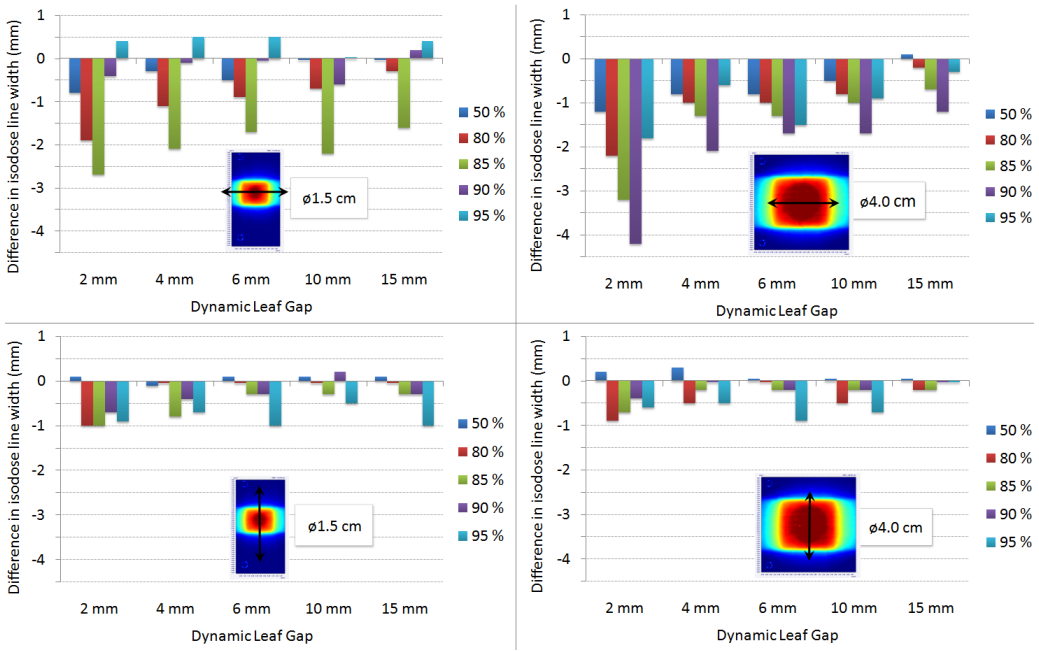

Figure 7-4. The difference in the measured peripheral doses of the tumours (SWA - 3D-CRT) with various widths of SWAs quantified by isodose line widths of 50%, 80%, 85%, 90% and 95%.

Isodose line widths of 50%, 80%, 85%, 90% and 95% were obtained from the film measurements and dose calculations to quantify the difference in surface doses from various SWAs. To be able to quantify the decrease in surface doses by a modulated field the open field irradiations of 3D-CRT were selected as a reference. The measurements revealed that the peripheral doses of the tumours were decreased as the SWA decreased. This can be seen from Figure 7-4. The largest difference in tumour peripheral doses was recorded in the direction of leaf movement (X-direction) with the Ø4.0 cm tumour with the smallest SWA (2 mm) as the isodose line width of 90% was 2 mm narrower than the open field treatment plan. This relates to a dose difference of

6%. The peripheral dose differences as a function of SWA were not modelled by the calculation algorithms.

7.3 IMRT optimization techniques

The ability of DABO to produce comparable dose distributions to standard IMRT optimization techniques with increased efficiency was investigated in (III). IMRT treatment plans were superior to 3D-CRT treatment plans by increasing PTV uniformity and coverage. With 3D-CRT the average SD and D95 values were 7.0 and 49.2 Gy while the average of the all IMRT treatment plans the corresponding values were 4.4 and 52.0 Gy. The prescription dose to the PTV was 56 Gy. The average maximum doses of the PTV were 111.1%, 109.3%, 111.4% and 108.0% for the 3D-CRT, DABO and standard SMLC and DMLC, respectively. The two SMLC techniques yielded comparable results in sparing of critical organs and PTV coverage. The values for the SD were 4.5 and 4.8 and for the D95 51.8 Gy and 51.9 Gy with the conventionally optimized SMLC and DABO, respectively. Target dose homogeneity and coverage were slightly better with DMLC (SD 3.9 and D95 52.3 Gy) than with SMLC.

The direct optimization was able to produce comparable target conformity when compared to conventional IMRT planning techniques with using just half of the apertures than the conventional SMLC (32 vs. 67). The average leaf width measured from the area of the PTV with DMLC, SMLC and DABO was 1.74 cm, 2.72 cm and 4.92 cm, respectively. The reduction in the number of apertures is illustrated in Figure 7-5, where the optimized leaf apertures from DABO and fluence based optimization is presented for the same field. As a result the number of MUs created by direct optimization was reduced by a factor of 2.3 and 1.8 when compared to conventional DMLC and SMLC, respectively. Interestingly, the number of MUs with DABO was 10% smaller than with 3D-CRT. This could be explained by the use of physical wedges in the treatments of 3D-CRT, which decrease the treatment efficiency by attenuating the primary beam.

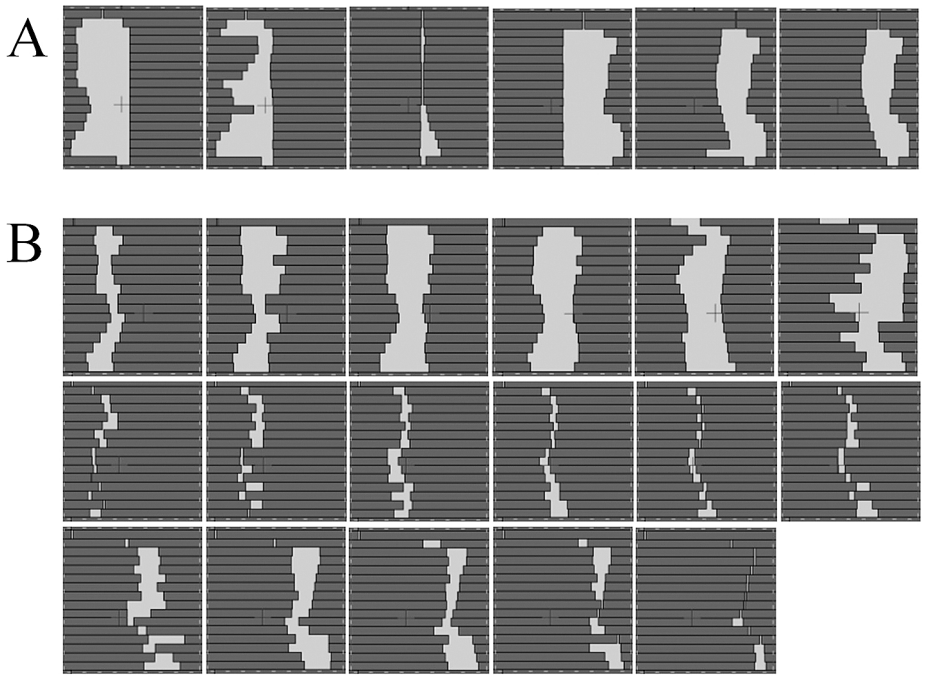

Figure 7-5. Optimized MLC apertures of DABO (A) and the corresponding SMLC apertures (B) for the same field.

The biological optimization process was investigated by DPBC with PCa (IV). The biological volumes were defined with ACE. The potential gain in dose escalation on biologically defined target volumes was estimated with TCP, NTCP and PUC. The probabilities of tumour control and complication of bladder and rectum were calculated for every treatment plan based on the DVH data. The mean TCP was lowest with the sIMRT plans (87.0%) and highest with the SIBIMRT 90 Gy plans (100.0%). With every patient the TCP was increased with SIBIMRT without increasing the complication probabilities of the bladder or rectum. The probability of tumour control of the BTV was increased on average by 12% (p-value < 0.022) with SIBIMRT when the same NTCP levels were selected as with the standard treatment plans. With SIBIMRT the PUC increased on average by 28% ($p < 0.0002$). The mean uncomplicated cure rate was 71.1% and 91.1% with sIMRT and SIBIMRT, respectively. By using biological optimization the highest PUC was obtained with an average dose of 82.1 Gy to the biologically defined volume. With the studied patients and the biological models the optimal dose of 82 Gy would have resulted on average a TCP 98.2% with a probability of 7.5% developing a complication (Grade II) of either bladder or rectum. The corresponding values with the standard IMRT treatment plans were 87.0% and 14.9%, respectively. The actual treatments of the studied PCa patients were carried out with the SIBIMRT technique such that the biologically defined target volume with a margin of 4 mm received a minimum dose of 80 Gy.

8 DISCUSSION

IMRT improves the dose coverage of the target volumes and can be use to enhance the sparing of critical organs when compared to 3D-CRT treatments. It is evident that a greater modulation in IMRT leads to better dose conformality. However, there is always a trade-off between the treatment plan quality and the required MUs needed to deliver the prescription dose. Compared to 3D-CRT the increased complexity is seen as decreased effective field size and an increase in MUs.

8.1 IMRT in CSI

Very long target volumes and the matching of cranial and spinal fields pose several challenges in the RT treatments of PNET. Accurate delivery of RT has a major role in the outcome of PNET but with 3D-CRT techniques it is extremely difficult to create a homogeneous dose to the whole PTV (Carrie et al 1999, Freeman et al 2002, Halperin 1996). In addition the interfraction feathering technique applied in 3D-CRT creates hot and cold spots to the spinal cord. The resulting dose distribution is also sensitive to the possible misalignment errors (Yom et al 2007). IMRT has already been used in CSI of the spinal axis and spinal-spinal junctions to increase the target volume homogeneity (Parker et al 2007). In the field junctions, however, a conventional field matching and the feathering technique were applied. Previously overlapping IMRT fields with intrafraction feathering in the spinal component of the treatment area have been utilized with two adjacent PA fields (Pai Panandiker et al 2007). However, the junction between the cranial and upper spinal field was executed conventionally with field matching. To our knowledge, the use of linac based IMRT in the treatment of the whole CSI with a single plan has not been reported before.

In (I) an IMRT technique was developed to enhance the dose homogeneity of the PTV in CSI. The dynamic sfIMRT technique was able to overcome the problem of field matching and was able to minimize the under and over dosage of the spinal cord. In the treatment of CSI a uniform dose distribution in spinal cord is very challenging to attain with the 3D-CRT technique. The average minimum dose delivered to the spinal cord was on average 79.1% of the prescription dose with 3D-CRT while with sfIMRT the corresponding dose was 91.7%. The split field technique showed also major improvement in dose uniformity within the whole PTV compared to the 3D-CRT treatment plans.

The major benefit of the dynamic intrafraction sfIMRT feathering technique is that the dose gradients are shallow in the junction areas and the total dose can be delivered with a single treatment plan. The resulting dose distributions are homogeneous and consequently the treatment plan is insensitive to misalignment errors. The split field technique was found to be insensitive to geographical uncertainties of the CSI treatment. With the ± 3 mm longitudinal error in treatment delivery the maximum dose error in the

spinal-spinal junction was 4% with sfIMRT and 37% with the 3D-CRT, respectively. However, the maximum error in the cranial-spinal junction was 11% with sfIMRT which could be decreased by increasing the overlapping areas of the adjacent fields, which were now the recommended minimum of 4 cm. The overlapping areas can be increased for example by using more beam directions to avoid the irradiation of mandible. With multiple beam directions the dose to other eloquent areas such as parotid glands, oesophagus and thyroid gland could also be decreased.

The drawback of sfIMRT delivery technique was the increase in the number of MUs needed to deliver the prescribed dose to the PTV. The number of MUs with a fraction dose of 1.8 Gy was on average 1170 MU with sfIMRT and 611 MU with 3D-CRT. Since the field directions were identical in the treatment plans of sfIMRT and 3D-CRT the volume irradiated was not increased and the only factor that affects the amount of peripheral doses was the increased collimator scatter and head leakage. Due to the decreased effective field size in sfIMRT the internal patient scatter could be lower than with the 3D-CRT but the increase in MUs will increase the amount of scattered radiation outside the treatment field. With direct aperture optimization, however, the number of MUs could be reduced and the risk of developing a second cancer could consequently be minimized.

8.2 IMRT in SLRT

Intensity map optimization techniques require a separate leaf sequencing algorithm to define the apertures that recreate the optimized beam intensities. To be able to fulfil the required intensities by moving or static MLC a large number of field shapes are often needed. The more complex and greater the intensity levels are the smaller are usually the field apertures. Very small apertures are highly sensitive to MLC positional errors and the dosimetric settings of the MLC. Also with small apertures the electronic equilibrium within the treatment field is not restored, which will cause rebuild-up and rebuild-down effects at the interfaces of low and high density material. The build-up effects are not modelled accurately by most of the current dose calculation algorithms in RT treatment planning. In (II) small lung tumour doses irradiated by intensity-modulated techniques were assessed to understand the risk for dose calculation errors in precision radiotherapy such as SLRT.

The effects of small dynamic apertures on the peripheral doses of small lung tumours have not been investigated earlier. A variety of measurements have been performed with conformal plans in phantoms simulating lung tumours (Dobler et al 2006, Panettieri et al 2007, Sikora et al 2009). Ong et al (2011) investigated dose distributions delivered with VMAT with film measurements in a lung phantom. The peripheral doses of the simulated tumour were not, however, investigated in the study. In (II) the width of the MLC leaf pairs was found to be proportional to the build-up doses in the vicinity of lung equivalent heterogeneities. The smaller the SWA, the bigger was the build-up region

at the lung-tumour interface. A more than 2 mm decrease in isodose line width was observed with SWAs of 2 mm and 4 mm. The decrease in tumour peripheral doses with a function of SWA was not modelled by the studied calculation algorithm of AAA or PBC. Surprisingly the maximum difference in isodose line width was smaller with the small tumour (2.6 mm) than with the large tumour (4.2 mm).

The studied type-a calculation algorithm (PBC) in (II) was able to model the dose accurately in the centre of the simulated large tumour surrounded by cork. However, the lack of accounting for the lateral electron transport in heterogeneous media led to overestimation of the calculated dose in the smaller tumour by over 5%. The type-b calculation algorithm (AAA) was able to calculate the central doses of both tumours accurately with conventional treatment fields (± 2%). The calculation accuracy was decreased by increasing the beam modulation and the differences were emphasized with the smaller tumour. The largest discrepancies were observed with the Ø1.5 cm tumour and with the smallest sliding windows (2 mm and 4 mm), where the AAA underestimated the dose delivered by 8% at maximum. The main reason for this discrepancy could be due to the rounded leaf end transmission (DLS) and leaf transmission values set in beam configuration. The values of DLS and transmission were optimized for conventional treatment plans and for the junction areas of dynamically split IMRT fields. The values of DLS and leaf transmission in (II) were 0.6 mm and 2.0%, respectively. Chang et al (2008) measured the DLS of the HD-MLC to be 0.84 mm for the energy of 6 MV with leaf leakage of 1.0%. It is evident that very small target volumes are sensitive to the dosimetric settings of the HD-MLC. The beam hardening effect becomes also more pronounced by decreasing the SWA which cannot be modelled in the Eclipse® beam configuration since it uses a constant-value model. However, when the target volume was larger (in this study Ø4.0 cm) the calculation errors decreased, although the percentage of dose coming from leaf transmission increased. Future studies of the discrepancies between the calculated and measured dose are required to minimize the dose calculation errors in small targets delivered with the HD-MLC.

There are possible two main reasons for the discrepancies between the more accurate type-b calculation algorithm (AAA) and measurements. The first is the limited accuracy of modelling the MLC transmission and leaf end curvature in the TPS only with two user defined parameters. The values of these parameters cannot be set to result in accurate dose calculations in all clinical situations ranging from very large split field IMRT techniques to very small treatment fields and leaf openings. The second reason could be that the IMRT dose distributions are calculated from the fluence distribution and not from the actual leaf positions. That is if the sliding window aperture creates a uniform field intensity the dose will be calculated as an open field.

The effect of beam modulation on the calculation accuracy was also observed in the RapidArc dose deliveries in (II). With greater beam intensity modulation the calculation accuracy decreased about 2% when compared to the “mildly” modulated arc delivery. Also with greater modulation the measured dose distribution was less homogeneous

than the calculated dose distribution. The explanation of this could potentially be the inaccurate modelling of the rounded leaf end transmission and the effect is increased as the aperture sizes are decreased. Fog et al (2011) observed the same effect with the RapidArc dose deliveries with a homogeneous phantom. They recorded dose calculation inaccuracies up to 20% with a small target volume (0.4 cm^3).

The value of DLS is determined for every energy and MLC during commissioning of the MLC and the calculation algorithm. The values of DLS not only depend on the leaf curvature of the MLC but also on the beam data configured, especially the width of the measured open beam penumbras. They account for the uncertainty of the defined DLS values and also emphasize the need to verify the calculated IMRT dose distributions with a variety of target volumes. The high deviation in the defined DLS (0.8 to 2.0 mm) by various authors (Chang et al 2008, Lee et al 2007, LoSasso et al 2008) underlines the need of an accurate determination of DLS by not just point measurements with a ionization chamber but rather extensive dose distribution measurements in 2D. The demand of more accurate dose calculation algorithms is also evident in the use of small apertures since the studied calculation algorithms (PBC and AAA) cannot model the MLC characteristics with just two user defined parameters. With more complex beam shaping the depth and field size dependence of MLC transmission, scatter properties and variation in beam penumbra with different leaf positions needs to be modelled more accurately to achieve high precision in the calculated dose. For example, it has been reported that the dynamic collimator scatter factors can vary from open field data by as much as 30% for 1 mm leaf gaps (Higgins and Alaei, 2006). As a result inadequate modelling of narrow apertures can cause major overdosage in the treated volumes. Based on the results of the study (II) the minimum aperture size should not be smaller than 6 mm in IMRT treatment delivery to achieve calculation accuracy of ± 4%.

8.3 Direct aperture based optimization

With the studied H&N patients in (III) the IMRT techniques yielded more uniform coverage of PTV than the 3D-CRT techniques. With respect to PTV coverage the DMLC technique performed slightly better than the SMLC delivery methods. The main drawback of the dynamic technique was the highest MUs among the evaluated techniques. Intensity map optimizations have a tendency to use a large number of complex field shapes in radiation beam delivery. The optimized fluence complexity, in terms of number of MUs and dynamic window width has correlated to accuracies of dose delivery when comparing calculated and delivered dose distributions (Giorgia et al 2007). Attempts to reduce the complexity of IMRT treatment plans have been conducted by using intensity limits and penalties or smoothing filters (Coselmon et al 2005, Giorgia et al 2007, Matuszak et al 2007). An alternative and efficient way to reduce the beam complexity and consequently increase the treatment efficiency is to use direct aperture based optimization methods (Bergman et al 2006, Li et al 2003, Shephard et al 2002). With direct optimization methods the MLC dependent constraints are included in the

optimization and intensity distributions as an intermediate step is not required. DABO method was presented in (III), where the number of MUs required achieving comparable dose distribution with commercial IMRT techniques was greatly reduced. The motivation to use direct optimization method in IMRT is to reduce the treatment time, scattered radiation and dose delivery inaccuracies by reducing the number of segments without degrading the dose distribution in the patient. With the studied DABO the MUs were reduced on average from the initial 683 MU to 379 MU and the number of apertures from 67 to 32. The efficiency of the treatment delivery was consequently increased by a factor of two, which is in line with other direct optimization methods (Bergman et al 2006, Li et al 2003, Shephard et al 2002). The target coverage and the normal tissue sparing were comparable between the studied DABO and conventional IMRT plans, respectively.

With increasing survival time of the patients, the risk of secondary malignancies needs to be lowered as much as possible. The introduction of IMRT requires an increase in the number of MUs delivered and consequently there is a risk of increasing the probability of second cancer with the increased peripheral doses. Although the latest studies have hypothesized that the RT treatment related second cancer risks outside the primary beams between 3D-CRT and IMRT is small (Bednarz et al 2010), the investigation in (III) supports the view that with the DABO technique the MUs and related risk of secondary malignancy can be kept at the level typical with 3D-CRT.

Available data suggests that a threshold of 0.6 Gy (and 0.1 Gy for children) for second primary malignancy after fractionated radiotherapy exists (Tubiana 2009). Out-of-field doses from the collimator scatter and head leakage start to dominate over patient scatter at distances over 15 cm from the field edge (Kry et al 2009). The measured and calculated doses at the distance of 15 cm from the edge of 10×10 cm^2 field are about 100 μGy with one MU delivered, about half originating from collimator scatter and head leakage (Kry et al 2009). With a typical IMRT H&N treatment plan the number of MUs delivered with one fraction is about 1000 MU. If for example 30 fractions would be delivered, this would result in a dose of 1.5 Gy with a distance of 15 cm from the field edge from the head leakage and collimator scatter. Based on the data of Kry et al (2009) at the distance of 40 cm from the field edge the corresponding approximation would be 0.4 Gy, which is four times larger than the speculated threshold dose of 0.1 Gy creating a second malignancy for children.

8.4 Biological treatment plan optimization

There is always a the trade-off between the treatment plan quality and the required amount of MUs needed to deliver the prescription dose and the possible reduction in MUs depends also on the complexity of the treated volume (Craft et al 2007). However, with DABO methods the effective field sizes can be increased without compromising the plan quality when compared to fluence based optimizations. By enabling the irradiation

with large aperture sizes the inaccuracies of calculation algorithms is also decreased. By increasing the effective field size the lateral electron disequilibrium is also decreased, which will enhance the calculation accuracy adjacent to low-density inhomogeneities. An important question is what exactly is an optimal treatment plan and are we able to define it for each individual patient? One approach to increase the therapeutic ratio and improve the "optimality" of a treatment plan would be the use of biological images and dose painting methods. Very important aspect of RT is to be able to define the areas of potential tumour cells with high accuracy. Unfortunately the existing imaging methods are not able to distinguish the individual cancer cells albeit may to some extent image the most radioresistant areas of the tumour spread. Dose painting can be applied to boost those most resistant areas to higher doses with the aim of increasing the TCP. By boosting only small volumes the normal tissue complications can be lowered or kept at the level of conventional treatments. In (IV) the potential of DPBC by dynamic IMRT delivery was investigated with 12 PCa patients. The motivation to study the possibility to use higher doses in the treatment of PCa was the knowledge that the recurrences after radiotherapy have been due to underdosage of the primary tumour area rather than geographical misses (Cellini et al 2002, Dearnaley et al 2005). However, if the dose to the whole prostate is increased the normal tissue toxicity is also increased unless the high dose volumes are decreased (Söhn et al 2007, van Lin et al 2006).

The feasibility of using functional MR imaging techniques to specify IPLs for the external beam RT treatment planning has already been studied (Fonteyne et al 2008, van Lin et al 2006). MRI or MRS images need to be usually fused with CT images and the possible changes in treatment anatomy between the images and the possible geometrical distortions in MR images can create inaccuracies in the treatments (Lian et al 2004). In (IV) PET/CT with ACE was utilized to delineate the IPLs. With a combined PET/CT image co registration is not needed because they share the same patient-based dicom-coordinates. However, the spatial resolution of PET is limited by the detector design and by the reconstruction process. The limited resolution will cause spillover and partial volume effects (PVE) and because of this a small source is imaged as a larger but dimmer source (Soret et al 2007). Because of the PVE of the PET/CT scanner the IPLs defined in (IV) are probably overestimated in size. This did not, however, diminish the ability to boost the volumes of the IPLs to higher and potentially more curative doses without increasing the NTCPs of the treatments.

In (IV) the normal tissue complication and tumour control probabilities were calculated with LKB- and ZM-models, respectively. Radiobiological parameters play an important role in biological optimization of treatment plans. In the TCP model the tumour clonogen density was presumed to be 1.6×10^6 cm^{-3}, the α/β value 3.1 Gy and the value of α 0.15 Gy^{-1} (Wang et al 2003b). With the selected values the SIBIMRT treatment delivery of 90 Gy would have resulted in 2 Gy equivalent dose of 95.8 Gy. Clinical studies have revealed that the α/β ratio of PCa could be as low as 1.5 Gy or as high as 4.96 Gy (Brenner and Hall 1999, Fowler et al 2001, King and Mayo 2000). Calculated 2 Gy equivalent

doses with these values would result in doses of 97.7 Gy and 94.7 Gy, respectively. This shows the effect on biologically equivalent dose by changing just one parameter with a moderately low uncertainty. The other biological model parameters have even higher degree of uncertainty than the extensively studied α/β ratio of PCa.

The incomplete knowledge of clinical data poses challenges in the clinical implementation of dose painting. Since individual patients have different radiosensitivities the TCP and NTCP estimations are more or less isoeffect calculations. Thus we can only compare the effectiveness between the different treatment plans. The models for the treatment outcome prediction also struggle with the uncertainties in radiosensitivity parameters which are mainly the number of clonogens, quantification of hypoxia, possible reoxygenation rate and the repopulation of the tumour cells. Clearly new patient specific methods and parameters in radiobiological models are also needed to relate the imaged biological data to the probability models.

The limitations of different imaging methods for biological adaptive-IMRT have to also be recognized. For example, the finite resolution of PET scanners will cause discrepancies between images and reality if the imaged regions are small and highly active (Christian et al 2009). DPBN or DPBC should therefore be carefully considered and should take these limitations into account.

In (IV) we showed that we are able to adapt RT to hypothetically more resistant tumour subvolumes but the question of defining the biological elements responsible for radioresistance remains. The variations in radiosensitivity can result from the differences in blood flow, hypoxia, proliferation, subpopulations with genetic mutations and number of stem cells. Optimally, the RT treatment planning should deliver the dose nonuniformly by taking into account the heterogeneity in radiosensitivity. The data is unfortunately sparse with high doses and the relation to normal tissue toxicity, the functional importance of different regions of organs, the variation in patient radiosensitivity and the effect of concurrent chemotherapy or antibody drugs. There is a clear need to relate the imaged information to the biological parameters in mathematical models since the employment of different biological models in the calculation of TCP and NTCP are only as accurate as the data variables applied to the models. The full implementation of patient-specific treatment planning will, however, require extensive clinical validation and probably more than a decade to develop (Stewart and Li, 2007). The future studies will further focus on the possibilities to define the biologically customized treatment plan for each patient based on the biological imaging and on the biological effectiveness of the given treatments.

9 CONCLUSIONS

The basic principle of IMRT is to modulate the treatment fields to achieve highest possible tumour coverage with minimal or acceptable normal tissue damage. The feasibility of dynamic split field IMRT technique was utilized to smooth sharp dose gradients in the junction areas of CSI (I). With the implemented sfIMRT technique the dose coverage of the PTV was increased without increasing normal tissue doses when compared to conventional 3D-CRT technique. The complexity of the treatment planning process was decreased and the safety of the treatments was increased with the sfIMRT by decreasing the steep dose gradients in the junction areas. The drawback for using IMRT in the CSI was the increase in MUs and treatment time due to decrease in effective field size. These factors have to be considered especially when treating paediatric patients since the incidence of second cancer might be increased due to increased collimator scatter and head leakage.

The possible limitations of using IMRT in small targets near inhomogeneities were studied in (II) with 6 MV photons. It was found with lung tumour simulating phantom that when decreasing the aperture size the rebuild-up and rebuild-down effects were increased as expected. This led to decreased peripheral dose of the mimicked tumours, which was not modelled with the investigated calculation algorithms. However, with an aperture width of 6 mm or more the difference in the surface doses between 3D-CRT and IMRT was found to be less than 3%.

One of the solutions to increase the effective size of the IMRT apertures would be the use of direct optimization of MLC. The decrease in field complexity would increase the efficiency of the IMRT treatments by decreasing the number of MUs needed to deliver the prescription dose to the patient. The direct optimization method was investigated as an alternative to the fluence based optimization algorithms (III). The feasibility of DABO was demonstrated with complex and concave treatment volumes of H&N cancers. The normal tissue sparing between the studied IMRT techniques were nearly equal. With DABO the MUs were comparable to the studied 3D-CRT technique whereas the fluence based optimization techniques required more than two-fold higher MUs to deliver the prescription dose. As a result the studied direct optimization decreased the complexity of the treatment and the aperture sizes were increased.

The possibility of IMRT to treat small biologically defined volumes simultaneously to higher radiation doses was studied in (IV). By using dose painting the TCPs were improved without increasing the NTCPs with every PCa patient studied. With the examined biological models the optimal dose to the BTV was on average 82.1 Gy. The PUC was increased on average by 28% by using the optimized dose. With the dose of 82.1 Gy the calculated probability of tumour control was increased from 87.0% to 98.2% and the probability of normal tissue toxicity was decreased from 14.9% to 7.5%, when SIBIMRT and sIMRT techniques were compared, respectively. This study motivates to

further improve the biological and functional imaging methods for better definition of the target volumes and to relate the imaged information to biological models to achieve optimal treatment outcomes with IMRT.

ACKNOWLEDGEMENTS

This work was carried out at the Department of Oncology of Turku University Hospital and at the Cancer Centre of Kuopio University Hospital during the years 2003 – 2012.

My deepest gratitude goes to my supervisors. I wish to thank Docent Jarmo Kulmala for the comprehensive guidance and encouragement throughout these years and for the great atmosphere in the working environment. It has been a real pleasure to be working with you with this project. Docent Tapani Lahtinen, thank you for mentoring me during the years and especially in the start of my career of medical physicist. Thank you for giving me the opportunity, the guidance and support. Your enthusiasm for science has been contagious. Professor Heikki Minn, thank you for your continuous support, encouragement and belief and thank you for introducing me to the world of PET.

I am extremely grateful for Professor Seppo Pyrhönen, Head of the Department of Oncology and Radiotherapy of Turku University Hospital and Professor Vesa Kataja, Head of Department of Kuopio University Hospital Cancer Centre, giving me the opportunity to use the facilities and providing me financial support from the EVO grant.

I thank the reviewers of this dissertation, Docent Mikko Tenhunen and Adjunct Professor Anders Ahnesjö for their constructive criticism and valuable comments.

I am deeply grateful also to my co-authors: colleague and dear friend Sami Suilamo Lic.Sc. for spending late hours on the linac and for the collaboration, Pekka Kolmonen Ph.D for the guidance in IMRT optimization and for developing the Pekos which I was privileged to examine clinically, Docent Paula Lindholm for the experienced clinical perspective and support, Eveliina Arponen M.Sc. for the knowledge of synthesis of carbon-11 acetate, Docent Marko Seppänen for the expertise in PET imaging, Pekka Mali M.D. for the experience and guidance in lung cancer.

Gore, Hege, Jussi and Twabne: Without the studies of basic physics I would not have written this thesis and without you guys the building of that foundation would have been tedious or even an uncompleted task. The memories last forever.

I thank a good friend Jukka Kaikkonen for the engineer's perspective and for the help in providing me details from the linear accelerator and the MLC. Thank you also for the refreshing conversations and for the hold'em moments.

The staff of Department of Oncology and Radiotherapy of Turku University Hospital, Turku PET centre and Kuopio University Hospital Cancer Centre are gratefully acknowledged and I wish to thank all the co-workers for the pleasant time I have been privileged to spent together.

I would also like to acknowledge the financial support I received from Turku University Hospital (EVO-funding) and the Cancer Society of Finland for the financial support during my study leave.

Finally, I wish to express my gratitude to my parents, Mirjami and Kari, for the continuous love and support. My dear brother Peter, thank you for the support throughout my life and being there and for the conversations, good, bad or ugly.

Last, but not least, I want to thank my beloved wife Kati and our sons Anton and Emil for their constant support and their love and patience during these years. Thank you for always being there when I need it the most.

Kuopio, May 2012

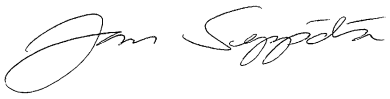

Jan Seppälä

REFERENCES

Aaltonen P, Brahme A, Lax I, Levernes S, Näslund I, Reitan JB, Turesson I. Specification of dose delivery in radiation therapy. Recommendations by the Nordic Association of Clinical Physics (NACP). Acta Oncol. 1997;36:S1-32.

Aarup LR, Nahum AE, Zacharatou C, Juhler-Nøttrup T, Knöös T, Nyström H, Specht L, Wieslander E and Korreman SS. The effect of different lung densities on the accuracy of various radiotherapy dose calculation methods: implications for tumour coverage. Radiother Oncol. 2009;91(3):405-14.

Agazaryan N, Solberg TD. Segmental and dynamic intensity-modulated radiotherapy delivery techniques for micro-multileaf collimator. Med Phys. 2003;30(7):1758-67.

Ahnesjö A, Aspradakis MM. Dose calculations for external photon beams in radiotherapy. Phys Med Biol. 1999;44(11):R99-155.

Ahunbay EE, Chen GP, Thatcher S, Jursinic PA, White J, Albano K, Li XA. Direct aperture optimization-based intensity-modulated radiotherapy for whole breast irradiation. Int J Radiat Oncol Biol Phys. 2007;67(4):1248-58.

Al-Mamgani A, Heemsbergen WD, Peeters ST, Lebesque JV. Role of intensity-modulated radiotherapy in reducing toxicity in dose escalation for localized prostate cancer. Int J Radiat Oncol Biol Phys. 2009;73(3):685-91.

Alaei P, Higgins PD, Weaver R, Nguyen N. Comparison of dynamic and step-and-shoot intensity-modulated radiation therapy planning and delivery. Med Dosim. 2004;29(1):1-6.

Alongi F, Fiorino C, Cozzarini C, Broggi S, Perna L, Cattaneo GM, Calandrino R, Di Muzio N. IMRT significantly reduces acute toxicity of whole-pelvis irradiation in patients treated with post-operative adjuvant or salvage radiotherapy after radical prostatectomy. Radiother Oncol. 2009;93(2):207-12.

Arbea L, Ramos LI, Martínez-Monge R, Moreno M and Aristu J. Intensity-modulated radiation therapy (IMRT) vs. 3D conformal radiotherapy (3DCRT) in locally advanced rectal cancer (LARC): dosimetric comparison and clinical implications. Radiat Oncol. 2010;5:17.

Athar BS, Paganetti H. Comparison of second cancer risk due to out-of-field doses from 6-MV IMRT and proton therapy based on 6 pediatric patient treatment plans. Radiother Oncol. 2011;98(1):87-92.

Baldock C, De Deene Y, Doran S, Ibbott G, Jirasek A, Lepage M, McAuley KB, Oldham M, Schreiner LJ. Polymer gel dosimetry. Phys Med Biol. 2010;55(5):R1-63.

Bednarz B, Athar B, Xu XG. A comparative study on the risk of second primary cancers in out-of-field organs associated with radiotherapy of localized prostate carcinoma using Monte Carlo-based accelerator and patient models. Med Phys. 2010;37(5):1987-94.

Behrens CF. Dose build-up behind air cavities for Co-60, 4, 6 and 8 MV. Measurements and Monte Carlo simulations. Phys Med Biol. 2006;51(22):5937-50.

Bentzen SM. Theragnostic imaging for radiation oncology: dose-painting by numbers. Lancet Oncol. 2005;6(2):112-7.

Bentzen SM, Constine LS, Deasy JO, Eisbruch A, Jackson A, Marks LB, Ten Haken RK, Yorke ED. Quantitative Analyses of Normal Tissue Effects in the Clinic (QUANTEC): an introduction to the scientific issues. Int J Radiat Oncol Biol Phys. 2010;76(3 Suppl):S3-9.

Bergman AM, Bush K, Milette M-P, Popescu IA, Otto K, Dunzenli C. Direct aperture optimization for IMRT using Monte Carlo generated beamlets. Med Phys. 2006;33(10):3666-79.

Bouchard H, Seuntjens J. Ionization chamber-based reference dosimetry of intensity modulated radiation beams. Med Phys. 2004;31(9):2454-65.

Bowen SR, Flynn RT, Bentzen SM, Jeraj R. On the sensitivity of IMRT dose optimization to the mathematical form of a biological imaging-based prescription function. Phys Med Biol. 2009;54(6):1483-501.

Bragg CM, Wingate K, Conway J. Clinical implications of the anisotropic analytical algorithm for IMRT treatment planning and verification. Radiother Oncol. 2008;86(2):276-84.

Brændengen M, Hansson K, Radu C, Siegbahn A, Jacobsson H, Glimelius B. Delineation of Gross Tumor Volume (GTV) for Radiation Treatment Planning of Locally Advanced Rectal Cancer Using Information From MRI or FDG-PET/CT: A Prospective Study. Int J Radiat Oncol Biol Phys. 2011;81(4):e439-45.

Brahme A. Optimization of stationary and moving beam radiation therapy techniques. Radiother Oncol. 1988;12(2):129-40.

Brenner DJ. Dose, volume and tumour control predictions in radiotherapy. Int J Radiat Oncol Biol Phys. 1993;26(1):171-9.

Brenner DJ, Curtis RE, Hall EJ, Ron E. Second malignancies in prostate carcinoma patients after radiotherapy compared with surgery. Cancer. 2000;88(2):398-406.

Brenner DJ, Hall EJ. Fractionation and protraction for radiotherapy of prostate carcinoma. Int J Radiat Oncol Biol Phys. 1999;43(5):1095-1101.

Brenner DJ, Hlatky LR, Hahnfeldt PJ, Huang Y, Sachs RK. The linear-quadratic model and most other common radiobiological models result in similar predictions of time-dose relationships. Radiat Res. 1998;150(1):83-91.

Bucciolini M, Buonamici FB, Mazzocchi S, De Angelis C, Onori S, Cirrone GA. Diamond detector versus silicon diode and ion chamber in photon beams of different energy and field size. Med Phys. 2003;30(8):2149-54.

Cahlon O, Hunt M, Zelefsky MJ. Intensity-modulated radiation therapy: supportive data for prostate cancer. Semin Radiat Oncol. 2008;18(1):48-57.

Carrasco P, Jornet N, Duch MA, Weber L, Ginjaume M, Eudaldo T, Jurado D, Ruiz A, Ribas M. Comparison of dose calculation algorithms in phantoms with lung equivalent heterogeneities under conditions of lateral electronic disequilibrium. Med Phys. 2004;31(10):2899-911.

Carrie C, Hoffstetter S, Gomez F, Moncho V, Doz F, Alapetite C, Murraciole X, Maire JP, Benhassel M, Chapet S, Quetin P, Kolodie H, Lagrange JL, Cuillere JC, Habrand JL. Impact of targeting deviations on outcome in medulloblastoma: study of the French Society of Pediatric Oncology (SFOP). Int J Radiat Oncol Biol Phys. 1999;45(2):435-9.

Cellini N, Morganti AG, Mattiucci GC, Valentini V, Leone M, Luzi S, Manfredi R, Dinapoli N, Digesu' C, Smaniotto D. Analysis of intraprostatic failures in patients treated with hormonal therapy and radiotherapy: implications for conformal therapy planning. Int J Radiat Oncol Biol Phys. 2002;53(3):595-9.

Chandraraj V, Stathakis S, Manickam R, Esquivel C, Supe SS, Papanikolaou N. Comparison of four commercial devices for RapidArc and sliding window IMRT QA. J Appl Clin Med Phys. 2011;12(2):338-49.

Chang SX, Cullip TJ, Deschesne KM, Miller EP, Rosenman JG. Compensators: an alternative IMRT delivery technique. J Appl Clin Med Phys. 2004;5(3):15-36.

Chang Z, Wang Z, Wu QJ, Yan H, Bowsher J, Zhang J, Yin FF. Dosimetric characteristics of Novalis Tx system with high definition multileaf collimator. Med Phys. 2008;35(10):4460-3.

Chao KS, Bosch WR, Mutic S, Lewis JS, Dehdashti F, Mintun MA, Dempsey JF, Perez CA, Purdy JA, Welch MJ. A novel approach to overcome hypoxic tumor resistance: Cu-ATSM-guided intensity-modulated radiation therapy. Int J Radiat Oncol Biol Phys. 2001;49(4):1171-82.

Chen SW, Yang SN, Liang JA, Shiau AC, Lin FJ. Comparative dosimetric study of two strategies of intensity-modulated radiotherapy in nasopharyngeal cancer. Med Dosim. 2005;30(4):219-27.

Chen GP, Ahunbay E, Schultz C, Li XA. Development of an inverse optimization package to plan nonuniform dose distributions based on spatially inhomogeneous radiosensitivity extracted from biological images. Med Phys. 2007;34(4):1198-205.

Chism DB, Horwitz EM, Hanlon AL, Pinover WH, Mitra RK, Hanks GE. Late morbidity profiles in prostate cancer patients treated to 79-84 Gy by a simple four-field coplanar beam arrangement. Int J Radiat Oncol Biol Phys. 2003;55(1):71-7.

Cho KH, Kim JY, Lee SH, Yoo H, Shin SH, Moon SH, Kim TH, Shin KH, Yoon M, Lee DH, Pyo HR. Simultaneous integrated boost intensity-modulated radiotherapy in patients with high-grade gliomas. Int J Radiat Oncol Biol Phys. 2010;78(2):390-7.

Christian JA, Bedford JL, Webb S, Brada M. Comparison of inverse-planned three-dimensional conformal radiotherapy and intensity-modulated radiotherapy for non-small-cell lung cancer. Int J Radiat Oncol Biol Phys. 2007;67(3):735-41.

Christian N, Lee JA, Bol A, De Bast M, Jordan B, Grégoire V. The limitation of PET imaging for biological adaptive-IMRT assessed in animal models. Radiother Oncol. 2009;91(1):101-6.

Chui CS, Chan MF, Yorke E, Spirou S, Ling CC. Delivery of intensity-modulated radiation therapy with a conventional multileaf collimator: comparison of dynamic and segmental methods. Med Phys. 2001;28(12):2441-9.

Chui CS, Spirou SV. Inverse planning algorithms for external beam radiation therapy. Med Dosim. 2001;26(2):189-97.

Clivio A, Fogliata A, Franzetti-Pellanda A, Nicolini G, Vanetti E, Wyttenbach R, Cozzi L. Volumetric-modulated arc radiotherapy for carcinomas of the anal canal: A treatment planning comparison with fixed field IMRT. Radiother Oncol. 2009;92(1):118-24.

Coselmon MM, Moran JM, Radawski JD, Fraass BA. Improving IMRT delivery efficiency using intensity limits during inverse planning. Med Phys. 2005;32(5):1234-45.

Cotrutz C, Xing L. Segment-based dose optimization using a genetic algorithm. Phys Med Biol. 2003;48(18):2987-98.

Cozzi L, Dinshaw KA, Shrivastava SK, Mahantshetty U, Engineer R, Deshpande DD, Jamema SV, Vanetti E, Clivio A, Nicolini G, Fogliata A. A treatment planning study comparing volumetric arc modulation with RapidArc and fixed field IMRT for cervix uteri radiotherapy. Radiother Oncol. 2008;89(2):180-91.

Cozzi L, Fogliata A, Bolsi A, Nicolini G, Bernier J. Three-dimensional conformal vs. intensity-modulated radiotherapy in head-and-neck cancer patients: comparative analysis of dosimetric and technical parameters. Int J Radiat Oncol Biol Phys. 2004;58(2):617-24.

Craft D, Süss P, Bortfeld T. The tradeoff between treatment plan quality and required number of monitor units in intensity-modulated radiotherapy. Int J Radiat Oncol Biol Phys. 2007;67(5):1596-605.

Das IJ, Ding GX, Ahnesjö A. Small fields: nonequilibrium radiation dosimetry. Med Phys. 2008;35(1):206-15.

Das S. A role for biological optimization within the current treatment planning paradigm. Med Phys. 2009;36(10):4672-82.

Davidson SE, Popple RA, Ibbott GS, Followill DS. Technical note: Heterogeneity dose calculation accuracy in IMRT: study of five commercial treatment planning systems using an anthropomorphic thorax phantom. Med Phys. 2008;35(12):5434-9.

Dawson A, Hillen T. Derivation of the tumour control probability (TCP) from a cell cycle model. Comput and Math Meth in Medicine. 2006;7:121-42.

Dearnaley DP, Hall E, Lawrence D, Huddart RA, Eeles R, Nutting CM, Gadd J, Warrington A, Bidmead M, Horwich A. Phase III pilot study of dose escalation using conformal radiotherapy in prostate cancer: PSA control and side effects. Br J Cancer. 2005;92(3):488-98.

Dearnaley DP, Sydes MR, Graham JD, Aird EG, Bottomley D, Cowan RA, Huddart RA, Jose CC, Matthews JH, Millar J, Moore AR, Morgan RC, Russell JM, Scrase CD, Stephens RJ, Syndikus I, Parmar MK; RT01 collaborators. Escalated-dose versus standard-dose conformal radiotherapy in prostate cancer: first results from the MRC RT01 randomised controlled trial. Lancet Oncol. 2007;8(6):475-87.

Deasy JO. Multiple local minima in radiotherapy optimization problems with dose-volume constraints. Med Phys. 1997;24(7):1157-61.

De Deene Y, Pittomvils G, Visalatchi S. The influence of cooling rate on the accuracy of normoxic polymer gel dosimeters. Phys Med Biol. 2007;52(10):2719-28.

De Gersem W, Claus F, De Wagter C, De Neve W. An anatomy-based beam segmentation tool for intensity-modulated radiation therapy and its application to head-and-neck cancer. Int J Radiat Oncol Biol Phys 2001;51(3):849–59.

De Ruysscher D, Faivre-Finn C, Nestle U, Hurkmans CW, Le Péchoux C, Price A, Senan S. European Organisation for Research and Treatment of Cancer recommendations for planning and delivery of high-dose, high-precision radiotherapy for lung cancer. J Clin Oncol. 2010;28(36):5301-10.

Dobler B, Walter C, Knopf A, Fabri D, Loeschel R, Polednik M, Schneider F, Wenz F, Lohr F. Optimization of extracranial stereotactic radiation therapy of small lung lesions using accurate dose calculation algorithms. Radiat. Oncol. 2006;1:45.

Dörr W, Herrmann TJ. Cancer induction by radiotherapy: dose dependence and spatial relationship to irradiated volume. Radiol Prot. 2002;22:A117–21.

Eade TN, Hanlon AL, Horwitz EM, Buyyounouski MK, Hanks GE, Pollack A. What dose of external-beam radiation is high enough for prostate cancer? Int J Radiat Oncol Biol Phys 2007;68(3):682-9.

Earl MA, Afghan MK, Yu CX, Jiang Z, Shepard DM. Jaws-only IMRT using direct aperture optimization. Med Phys. 2007;34(1):307-14.

Eisbruch A, Schwartz M, Rasch C, Vineberg K, Damen E, Van As CJ, Marsh R, Pameijer FA, Balm AJ. Dysphagia and aspiration after chemoradiotherapy for head-and-neck cancer: which anatomic structures are affected and can they be spared by IMRT? Int J Radiat Oncol Biol Phys. 2004;60(5):1425-39.

Eklund K, Ahnesjö A. Spectral perturbations from silicon diode detector encapsulation and shielding in photon fields. Med Phys. 2010;37(11):6055-60.

Elliott SP, Jarosek SL, Alanee SR, Konety BR, Dusenbery KE, Virnig BA. Three-dimensional external beam radiotherapy for prostate cancer increases the risk of hip fracture. Cancer. 2011;117(19):4557-65.

Engelsman M, Damen EM, Koken PW, van ‘t Veld AA, van Ingen KM, Mijnheer BJ. Impact of simple tissue inhomogeneity correction algorithms on conformal radiotherapy of lung tumours. Radiother Oncol. 2001;60(3):299-309.

Fenoglietto P, Laliberte B, Allaw A, Ailleres N, Idri K, Hay MH, Moscardo CL, Gourgou S, Dubois JB, Azria D. Persistently better treatment planning results of intensity-modulated (IMRT) over conformal radiotherapy (3D-CRT) in prostate cancer patients with significant variation of clinical target volume and/or organs-at-risk. Radiother Oncol. 2008;88(1):77-87.

Fog LS, Rasmussen JF, Aznar M, Kjær-Kristoffersen F, Vogelius IR, Engelholm SA, Bangsgaard JP. A closer

look at RapidArc® radiosurgery plans using very small fields. Phys Med Biol 2011;56(6):1853-63.

Fogliata A, Vanetti E, Albers D, Brink C, Clivio A, Knöös T, Nicolini G, Cozzi L. On the dosimetric behaviour of photon dose calculation algorithms in the presence of simple geometric heterogeneities: comparison with Monte Carlo calculations. Phys Med Biol 2007;52(5):1363-85.

Fontenot JD, King ML, Johnson SA, Wood CG, Price MJ, Lo KK. Single-arc volumetric-modulated arc therapy can provide dose distributions equivalent to fixed-beam intensity-modulated radiation therapy for prostatic irradiation with seminal vesicle and/or lymph node involvement. Br J Radiol. 2011;28: In press.

Fonteyne V, Villeirs G, Speleers B, De Neve W, De Wagter C, Lumen N, De Meerleer G. Intensity-modulated radiotherapy as primary therapy for prostate cancer: report on acute toxicity after dose escalation with simultaneous integrated boost to intraprostatic lesion. Int J Radiat Oncol Biol Phys. 2008;72(3):799-807.

Fotina I, Winkler P, Künzler T, Reiterer J, Simmat I, Georg D. Advanced kernel methods vs. Monte Carlo-based dose calculation for high energy photon beams. Radiother Oncol. 2009;93(3):645-53.

Fowler JF. The linear-quadratic formula and progress in fractionated radiotherapy. Br J Radiol. 1989;62(740):679-94.

Fowler J, Chappell R, Ritter M. Is alpha/beta for prostate tumors really low? Int J Radiat Oncol Biol Phys. 2001;50(4):1021-31.

Fowler JF, Welsh JS, Howard SP. Loss of biological effect in prolonged fraction delivery. Int J Radiat Oncol Biol Phys. 2004;59(1):242-9.

Freeman CR, Taylor RE, Kortmann RD, Carrie C. Radiotherapy for medulloblastoma in children: a perspective on current international clinical research efforts. Med Pediatr Oncol. 2002;39(2):99-108.

Fuss M, Sturtewagen E, De Wagter C, Georg D. Dosimetric characterization of GafChromic EBT film and its implication on film dosimetry quality assurance. Phys Med Biol. 2007;52(14):4211-25.

Giorgia N, Antonella F, Eugenio V, Alessandro C, Filippo A, Luca C. What is an acceptably smoothed fluence? Dosimetric and delivery considerations for dynamic sliding window IMRT. Radiat Oncol. 2007;2:42.

Gomez D, Cahlon O, Mechalakos J, Lee N. An investigation of intensity-modulated radiation therapy versus conventional two-dimensional and 3D-conformal radiation therapy for early stage larynx cancer. Radiat Oncol. 2010;5:74.

Griessbach I, Lapp M, Bohsung J, Gademann G, Harder D. Dosimetric characteristics of a new unshielded silicon diode and its application in clinical photon and electron beams. Med Phys. 2005;32(12):3750-4.

Guckenberger M, Richter A, Krieger T, Wilbert J, Baier K, Flentje M. Is a single arc sufficient in volumetric-modulated arc therapy (VMAT) for complex-shaped target volumes? Radiother Oncol. 2009;93(2):259-65.

Guerrero M, Li XA, Ma L, Linder J, Deyoung C, Erickson B. Simultaneous integrated intensity-modulated radiotherapy boost for locally advanced gynecological cancer: radiobiological and dosimetric considerations. Int J Radiat Oncol Biol Phys. 2005;62(3):933-9.

Hall J, Wuu S. Radiation induced second cancers: the impact of 3D-CRT and IMRT. Int J Radiat Oncol Biol Phys 2003;56(1):83-8.

Halperin EC. Impact of radiation technique upon the outcome of treatment for medulloblastoma. Int J Radiat Oncol Biol Phys. 1996;36(1):233-9.

Halperin EC, Perez CA, Brady LW, Wazer DE, Freeman C, Prosnitz LR. Perez and Brady's Principles and Practice of Radiation Oncology. 5th Edition. 2007. Lippincott, Williams and Wilkins.

Higgins PD, Alaei P. Dose uncertainty due to aperture effects in dynamic fields. Med Phys. 2006;33(7):2418-25.

Hillen T, de Vries G, Gong J, Finlay C. From cell population models to tumor control probability: including cell cycle effects. Acta Oncol. 2010;49(8):1315-23.

Horiot JC, Le Fur R, N'Guyen T, Chenal C, Schraub S, Alfonsi S, Gardani G, Van Den Bogaert W, Danczak S, Bolla M, et al. Hyperfractionation versus conventional fractionation in oropharyngeal carcinoma: final analysis of a randomized trial of the EORTC cooperative group of radiotherapy. Radiother Oncol. 1992;25(4):231-41.

Hunt MA, Desobry GE, Fowble B, Coia LR. Effect of low-density lateral interfaces on soft-tissue doses. Int J Radiat Oncol Biol Phys. 1997;37(2):475-82.

Jabbari S, Kim HM, Feng M, Lin A, Tsien C, Elshaikh M, Terrel JE, Murdoch-Kinch C, Eisbruch A. Matched case-control study of quality of life and xerostomia after intensity-modulated radiotherapy or standard radiotherapy for head-and-neck cancer: initial report. Int J Radiat Oncol Biol Phys. 2005;63(3):725-31.

Jackson A, Kutcher GJ, Yorke ED. Probability of radiation-induced complications for normal tissues with parallel architecture subject to non-uniform irradiation. Med Phys. 1993;20(3):613-25.

Joiner MC, Mogili N, Marples B, Burmeister J. Significant dose can be lost by extended delivery times in IMRT with x rays but not high-LET radiations. Med Phys. 2010;37(6):2457-65.

Jones AO, Das IJ. Comparison of inhomogeneity correction algorithms in small photon fields. Med Phys. 2005;32(3):766-76.

Jones S, Williams M. Clinical evaluation of direct aperture optimization when applied to head-and-neck IMRT. Med Dosim. 2008;33(1):86-92.

Jothybasu KS, Bahl A, Subramani V, Rath GK, Sharma DN, Julka PK. Static versus dynamic intensity-modulated radiotherapy: Profile of integral dose in carcinoma of the nasopharynx. J Med Phys. 2009;34(2):66-72.

Keall PJ, Siebers JV, Jeraj R, Mohan R. The effect of dose calculation uncertainty on the evaluation of radiotherapy plans. Med Phys. 2000;27(3):478-84.

Kim Y, Tomé WA. Dose-painting IMRT optimization using biological parameters. Acta Oncol. 2010;49(8):1374-84

King CR, Mayo CS. Is the prostate α/β ratio of 1.5 from Brenner & Hall a modeling artifact? Int J Radiat Oncol Biol Phys. 2000;47(2):536-8.

Kirkpatrick S, Gelatt CD Jr, Vecchi MP. Optimization by simulated annealing. Science. 1983;220(4598):671-80.

Kirkpatrick JP, van der Kogel AJ, Schultheiss TE. Radiation dose-volume effects in the spinal cord. Int J Radiat Oncol Biol Phys. 2010;76:S42-9.

Knöös T, Wieslander E, Cozzi L, Brink C, Fogliata A, Albers D, Nyström H, Lassen S. Comparison of dose calculation algorithms for treatment planning in external photon beam therapy for clinical situations. Phys Med Biol. 2006;51(22):5785-807.

Kolmonen P. The direct control of the multi-leaf collimator in the inverse problem of radiotherapy treatment planning. PhD thesis 2004; University of Kuopio, Finland.

Kolmonen P, Tervo J, Lahtinen T. Use of the Cimmino algorithm and continuous approximation for the dose deposition kernel in the inverse problem of radiation treatment planning. Phys Med Biol. 1998;43:2539-54.

Koshy M, Paulino AC, Marcus RB Jr, Ting J. The effect of an extended source-to-skin distance in the treatment of the spinal field in children receiving craniospinal irradiation. Med Dosim. 2004;29:7-10.

Kry SF, Titt U, Pönisch F, Vassiliev ON, Salehpour M, Gillin M, Mohan R. Reduced neutron production through use of a flattening-filter-free accelerator. Int J Radiat Oncol Biol Phys. 2007;68(4):1260-4.

Kry SF, Salehpour M, Titt U, White RA, Stovall M, Followill D. Monte Carlo study shows no significant difference in second cancer risk between 6- and 18-MV intensity-modulated radiation therapy. Radiother Oncol. 2009;91(1):132-7.

Kuban DA, Tucker SL, Dong L, Starkschall G, Huang EH, Cheung MR, Lee AK, Pollack A. Long-term results of the M. D. Anderson randomized dose-escalation trial for prostate cancer. Int J Radiat Oncol Biol Phys. 2008;70(1):67-74.

Kupelian PA, Ciezki J, Reddy CA, Klein EA, Mahadevan A. Effect of increasing radiation doses on local and distant failures in patients with localized prostate cancer. Int J Radiat Oncol Biol Phys. 2008;71(1):16-22.

Kuperman VY, Ventura AM, Sommerfeldt M. Effect of radiation protraction in intensity-modulated radiation therapy with direct aperture optimization: a phantom study. Phys Med Biol. 2008;53(12):3279-92.

Kutcher GJ, Burman C, Brewster L, Goitein M, Mohan R. Histogram reduction method for calculating complication probabilities for three-dimensional treatment planning evaluations. Int J Radiat Oncol Biol Phys. 1991;21(1):137-46.

Källman P, Ågren A, Brahme A. Tumour and normal tissue responses to fractionated non-uniform dose delivery. Int J Radiat Biol. 1992;62(2):249-62.

Lamers-Kuijper E, Heemsbergen W, van Mourik A, Rasch C. Sequentially delivered boost plans are superior to simultaneously delivered plans in head and neck cancer when the boost volume is located further away from the parotid glands. Radiother Oncol. 2011;98(1):51-6.

Lauve A, Morris M, Schmidt-Ullrich R, Wu Q, Mohan R, Abayomi O, Buck D, Holdford D, Dawson K, Dinardo L, Reiter E. Simultaneous integrated boost intensity-modulated radiotherapy for locally advanced head-and-neck squamous cell carcinomas: II--clinical results. Int J Radiat Oncol Biol Phys. 2004;60(2):374-87.

Lee JW, Choi KS, Hong S, Kim YL, Chung JB, Lee DH, Choe BY, Jang HS, Suh TS. Effects of static dosimetric leaf gap on MLC-based small-beam dose distribution for intensity-modulated radiosurgery. J Appl Clin Med Phys. 2007;8(4):2397.

Lee TF, Chao PJ, Ting HM, Lo SH, Wang YW, Tuan CC, Fang FM, Su TJ. Comparative analysis of SmartArc-based dual arc volumetric-modulated arc radiotherapy (VMAT) versus intensity-modulated radiotherapy (IMRT) for nasopharyngeal carcinoma. J Appl Clin Med Phys. 2011;12(4):158-174.

Li XA, Wang JZ, Jursinic PA, Lawton CA, Wang D. Dosimetric advantages of IMRT simultaneous

integrated boost for high-risk prostate cancer. Int J Radiat Oncol Biol Phys. 2005;61(4):1251-7.

Li Y, Yao J, Yao D. Genetic algorithm based deliverable segments optimization for static intensity-modulated radiotherapy. Phys Med Biol. 2003;48(20):3353–74.

Lian J, Xing L, Hunjan S, Dumoulin C, Levin J, Lo A, Watkins R, Rohling K, Giaquinto R, Kim D, Spielman D, Daniel B. Mapping of the prostate in endorectal coil-based MRI/MRSI and CT: a deformable registration and validation study. Med Phys. 2004;31(11):3087-94.

Liao ZX, Komaki RR, Thames HD Jr, Liu HH, Tucker SL, Mohan R, Martel MK, Wei X, Yang K, Kim ES, Blumenschein G, Hong WK, Cox JD. Influence of technologic advances on outcomes in patients with unresectable, locally advanced non-small-cell lung cancer receiving concomitant chemoradiotherapy. Int J Radiat Oncol Biol Phys. 2010;76(3):775-81.

Lin Z, Mechalakos J, Nehmeh S, Schoder H, Lee N, Humm J, Ling CC. The influence of changes in tumor hypoxia on dose-painting treatment plans based on 18F-FMISO positron emission tomography. Int J Radiat Oncol Biol Phys. 2008;70(4):1219-28.

Ling CC, Humm J, Larson S, Amols H, Fuks Z, Leibel S, Koutcher JA. Towards multidimensional radiotherapy (MD-CRT): biological imaging and biological conformality. Int J Radiat Oncol Biol Phys. 2000;47(3):551-60.

Ling CC, Gerweck LE, Zaider M, Yorke E. Dose-rate effects in external beam radiotherapy redux. Radiother Oncol. 2010;95(3):261-8.

Liu HH, Wang X, Dong L, Wu Q, Liao Z, Stevens CW, Guerrero TM, Komaki R, Cox JD, Mohan R. Feasibility of sparing lung and other thoracic structures with intensity-modulated radiotherapy for non-small-cell lung cancer. Int J Radiat Oncol Biol Phys. 2004;58(4):1268-79.

Lohr F, El-Haddad M, Dobler B, Grau R, Wertz HJ, Kraus-Tiefenbacher U, Steil V, Madyan YA, Wenz F. Potential effect of robust and simple IMRT approach for left-sided breast cancer on cardiac mortality. Int J Radiat Oncol Biol Phys. 2009;74(1):73-80.

Longobardi B, De Martin E, Fiorino C, Dell'oca I, Broggi S, Cattaneo GM, Calandrino R. Comparing 3DCRT and inversely optimized IMRT planning for head and neck cancer: equivalence between step-and-shoot and sliding window techniques. Radiother Oncol. 2005;77(2):148-56.

Lorenz F, Nalichowski A, Rosca F, Kung J, Wenz F, Zygmanski P. Spatial dependence of MLC transmission in IMRT delivery. Phys Med Biol. 2007;52(19):5985-99.

LoSasso T, Chui CS, Ling CC. Physical and dosimetric aspects of a multileaf collimation system used in the dynamic mode for implementing intensity modulated radiotherapy. Med Phys. 1998;25(10):1919-27.

Losasso T. IMRT delivery performance with a varian multileaf collimator. Int J Radiat Oncol Biol Phys. 2008;71:S85-8.

Low DA, Moran JM, Dempsey JF, Dong L, Oldham M. Dosimetry tools and techniques for IMRT. Med Phys. 2011;38(3):1313-38.

Luxton G, Keall PJ, King CR. A new formula for normal tissue complication probability (NTCP) as a function of equivalent uniform dose (EUD). Phys Med Biol. 2008;53(1):23-36.

Lydon JM. Theoretical and experimental validation of treatment planning for narrow MLC defined photon fields. Phys Med Biol. 2005;50(11):2701-14.

Lyman JT. Complication probability as assessed from dose-volume histograms. Radiat Res. 1985;104:S13–9.

Mackay RI, Hendry JH. The modelled benefits of individualizing radiotherapy patients' dose using cellular radiosensitivity assays with inherent variability. Radiother Oncol. 1999;50(1):67-75.

Malhotra HK, Raina S, Avadhani JS, deBoer S, Podgorsak MB. Technical and dosimetric considerations in IMRT treatment planning for large target volumes. J Appl Clin Med Phys. 2005;6(4):77-87.

Malinen E, Søvik A, Hristov D, Bruland ØS, Olsen DR. Adapting radiotherapy to hypoxic tumours. Phys Med Biol. 2006;51(19):4903-21.

Marks LB, Bentzen SM, Deasy JO, Kong FM, Bradley JD, Vogelius IS, El Naqa I, Hubbs JL, Lebesque JV, Timmerman RD, Martel MK, Jackson A. Radiation dose-volume effects in the lung. Int J Radiat Oncol Biol Phys. 2010;76(3 Suppl):S70-6.

Matuszak MM, Larsen EW, Fraass BA. Reduction of IMRT beam complexity through the use of beam modulation penalties in the objective function. Med Phys. 2007;34(2):507-20.

Maule M, Scélo G, Pastore G, Brennan P, Hemminki K, Tracey E, Sankila R, Weiderpass E, Olsen JH, McBride ML, Brewster DH, Pompe-Kirn V, Kliewer EV, Chia KS, Tonita JM, Martos C, Jonasson JG, Merletti F, Boffetta P. Risk of second malignant neoplasms after childhood leukemia and lymphoma: an international study. J Natl Cancer Inst. 2007;99(10):790-800.

McDonald MW, Godette KD, Whitaker DJ, Davis LW, Johnstone PA. Three-year outcomes of breast intensity-modulated radiation therapy with

simultaneous integrated boost. Int J Radiat Oncol Biol Phys. 2010;77(2):523-30.

McGrath SD, Matuszak MM, Yan D, Kestin LL, Martinez AA, Grills IS. Volumetric modulated arc therapy for delivery of hypofractionated stereotactic lung radiotherapy: A dosimetric and treatment efficiency analysis. Radiother Oncol. 2010;95(2):153-7.

Meijer G, Steenhuijsen J, Bal M, De Jaeger K, Schuring D, Theuws J. Dose painting by contours versus dose painting by numbers for stage II/III lung cancer: practical implications of using a broad or sharp brush. Radiother Oncol. 2011;100(3):396-401.

Metwaly M, Awaad AM, El-Sayed el-SM, Sallam AS. Comparison of intensity-modulated radiotherapy and forward-planning dynamic arc therapy techniques for prostate cancer. J Appl Clin Med Phys. 2008;9(4):37-56.

Michalski JM, Klein EE, Gerber R. Method to plan, administer, and verify supine craniospinal irradiation. J Appl Clin Med Phys. 2002;3:310-6.

Mihaylov IB, Lerma FA, Wu Y, Siebers JV. Analytic IMRT dose calculations utilizing Monte Carlo to predict MLC fluence modulation. Med Phys. 2006;33(4):828-39.

Murshed H, Liu HH, Liao Z, Barker JL, Wang X, Tucker SL, Chandra A, Guerrero T, Stevens C, Chang JY, Jeter M, Cox JD, Komaki R, Mohan R. Dose and volume reduction for normal lung using intensity-modulated radiotherapy for advanced-stage non-small-cell lung cancer. Int J Radiat Oncol Biol Phys. 2004;58(4):1258-67.

Nelms BE, Rasmussen KH, Tomé WA. Evaluation of a fast method of EPID-based dosimetry for intensity-modulated radiation therapy. J Appl Clin Med Phys. 2010;11(2):140-57.

Nguyen F, Rubino C, Guerin S, Diallo I, Samand A, Hawkins M, Oberlin O, Lefkopoulos D, De Vathaire F. Risk of a second malignant neoplasm after cancer in childhood treated with radiotherapy: correlation with the integral dose restricted to the irradiated fields. Int J Radiat Oncol Biol Phys. 2008;70(3):908-15.

Nicolini G, Fogliata A, Cozzi L. IMRT with the sliding window: comparison of the static and dynamic methods. Dosimetric and spectral analysis. Radiother Oncol. 2005;75(1):112-9.

Niemierko A. Reporting and analyzing dose distributions: a concept of equivalent uniform dose. Med Phys. 1997;24(1):103-10.

Niyazi M, Bartenstein P, Belka C, Ganswindt U. Choline PET based dose-painting in prostate cancer--modelling of dose effects. Radiat Oncol. 2010;5:23.

Nutting CM, Morden JP, Harrington KJ, Urbano TG, Bhide SA, Clark C, Miles EA, Miah AB, Newbold K, Tanay M, Adab F, Jefferies SJ, Scrase C, Yap BK, A'Hern RP, Sydenham MA, Emson M, Hall E; PARSPORT trial management group. Parotid-sparing intensity modulated versus conventional radiotherapy in head and neck cancer (PARSPORT): a phase 3 multicentre randomised controlled trial. Lancet Oncol. 2011;12(2):127-36.

Nyandoto P, Muhonen T, Joensuu H. Second cancer among long-term survivors from Hodgkin's disease. Int J Radiat Oncol Biol Phys. 1998;42(2):373-8.

Oinam AS, Singh L. Verification of IMRT dose calculations using AAA and PBC algorithms in dose buildup regions. J Appl Clin Med Phys. 2010;11(4):105-21.

Olafsson A, Jeraj R, Wright SJ. Optimization of intensity-modulated radiation therapy with biological objectives. Phys Med Biol. 2005;50(22):5357-79.

Oldham M, Webb S. Intensity-modulated radiotherapy by means of static tomotherapy: a planning and verification study. Med Phys. 1997;24(6):827-36.

Ong C, Verbakel WF, Cuijpers JP, Slotman BJ, Senan S. Dosimetric impact of interplay effect on RapidArc lung stereotactic treatment delivery. Int J Radiat Oncol Biol Phys. 2011;79(1):305-11.

Orlandi E, Palazzi M, Pignoli E, Fallai C, Giostra A, Olmi P. Radiobiological basis and clinical results of the simultaneous integrated boost (SIB) in intensity modulated radiotherapy (IMRT) for head and neck cancer: A review. Crit Rev Oncol Hematol. 2010;73(2):111-25.

O'Rourke SF, McAneney H, Hillen T. Linear quadratic and tumour control probability modelling in external beam radiotherapy. J Math Biol. 2009;58(4-5):799-817.

Ottosson RO, Karlsson A, Behrens CF. Pareto front analysis of 6 and 15 MV dynamic IMRT for lung cancer using pencil beam, AAA and Monte Carlo. Phys Med Biol. 2010;55(16):4521-33.

Overgaard J, Mohanti BK, Begum N, Ali R, Agarwal JP, Kuddu M, Bhasker S, Tatsuzaki H, Grau C. Five versus six fractions of radiotherapy per week for squamous-cell carcinoma of the head and neck (IAEA-ACC study): a randomised, multicentre trial. Lancet Oncol. 2010;11(6):553-60.

Pai Panandiker A, Ning H, Likhacheva A, Ullman K, Arora B, Ondos J, Karimpour S, Packer R, Miller R, Citrin D. Craniospinal irradiation with spinal IMRT to improve target homogeneity. Int J Radiat Oncol Biol Phys. 2007;68(5):1402-9.

Panettieri V, Wennberg B, Gagliardi G, Duch MA, Ginjaume M, Lax I. SBRT of lung tumours:

Monte Carlo simulation with PENELOPE of dose distributions including respiratory motion and comparison with different treatment planning systems. Phys Med Biol. 2007;52(14):4265-81.

Palma D, Vollans E, James K, Nakano S, Moiseenko V, Shaffer R, McKenzie M, Morris J, Otto K. Volumetric modulated arc therapy for delivery of prostate radiotherapy: comparison with intensity-modulated radiotherapy and three-dimensional conformal radiotherapy. Int J Radiat Oncol Biol Phys. 2008;72(4):996-1001.

Pappas E, Maris TG, Zacharopoulou F, Papadakis A, Manolopoulos S, Green S, Wojnecki C. Small SRS photon field profile dosimetry performed using a PinPoint air ion chamber, a diamond detector, a novel silicon-diode array (DOSI), and polymer gel dosimetry. Analysis and intercomparison. Med Phys. 2008;35(10):4640-8.

Parker WA, Freeman CR. A simple technique for craniospinal radiotherapy in the supine position. Radiother Oncol. 2006;78(2):217-22.

Parker W, Filion E, Roberge D, Freeman CR. Intensity-modulated radiotherapy for craniospinal irradiation: target volume considerations, dose constraints, and competing risks. Int J Radiat Oncol Biol Phys. 2007;69(1):251-7.

Partridge M, Trapp JV, Adams EJ, Leach MO, Webb S, Seco J. An investigation of dose calculation accuracy in intensity-modulated radiotherapy of sites in the head & neck. Phys Med. 2006;22(3):97-104.

Peñagarícano JA, Papanikolaou N, Yan Y, Youssef E, Ratanatharathorn V. Feasibility of cranio-spinal axis radiation with the Hi-Art tomotherapy system. Radiother Oncol. 2005;76(1):72-8.

Peponi E, Glanzmann C, Willi B, Huber G, Studer G. Dysphagia in head and neck cancer patients following intensity modulated radiotherapy (IMRT). Radiat Oncol. 2011;6:1.

Petit SF, Dekker AL, Seigneuric R, Murrer L, van Riel NA, Nordsmark M, Overgaard J, Lambin P, Wouters BG. Intra-voxel heterogeneity influences the dose prescription for dose-painting with radiotherapy: a modelling study. Phys Med Biol. 2009;54(7):2179-96.

Petoukhova AL, van Wingerden K, Wiggenraad RG, van de Vaart PJ, van Egmond J, Franken EM, van Santvoort JP. Verification measurements and clinical evaluation of the iPlan RT Monte Carlo dose algorithm for 6 MV photon energy. Phys Med Biol. 2010;55(16):4601-14.

Petsuksiri J, Sermsree A, Thephamongkhol K, Keskool P, Thongyai K, Chansilpa Y, Pattaranutaporn P. Sensorineural hearing loss after concurrent chemoradiotherapy in nasopharyngeal cancer patients. Radiat Oncol. 2011;6:19.

Popple RA, Ove R, Shen S. Tumor control probability for selective boosting of hypoxic subvolumes, including the effect of reoxygenation. Int J Radiat Oncol Biol Phys. 2002;54(3):921-7.

Poppe B, Djouguela A, Blechschmidt A, Willborn K, Rühmann A, Harder D. Spatial resolution of 2D ionization chamber arrays for IMRT dose verification: single-detector size and sampling step width. Phys Med Biol. 2007;52(10):2921-35.

Pow EH, Kwong DL, McMillan AS, Wong MC, Sham JS, Leung LH, Leung WK. Xerostomia and quality of life after intensity-modulated radiotherapy vs. conventional radiotherapy for early-stage nasopharyngeal carcinoma: initial report on a randomized controlled clinical trial. Int J Radiat Oncol Biol Phys. 2006;66(4):981-91.

Price SJ, Jena R, Burnet NG, Hutchinson PJ, Dean AF, Peña A, Pickard JD, Carpenter TA, Gillard JH. Improved delineation of glioma margins and regions of infiltration with the use of diffusion tensor imaging: an image-guided biopsy study. AJNR Am J Neuroradiol. 2006;27(9):1969-74.

Qi XS, Semenenko VA, Li XA. Improved critical structure sparing with biologically based IMRT optimization. Med Phys. 2009;36(5):1790-9.

Richley L, John AC, Coomber H, Fletcher S. Evaluation and optimization of the new EBT2 radiochromic film dosimetry system for patient dose verification in radiotherapy. Phys Med Biol. 2010;55(9):2601-17.

Ruben JD, Lancaster CM, Jones P, Smith RL. A Comparison of Out-of-Field Dose and Its Constituent Components for Intensity-Modulated Radiation Therapy Versus Conformal Radiation Therapy: Implications for Carcinogenesis. Int J Radiat Oncol Biol Phys. 2011;81(5):1458-64.

Rubino C, Adjadj E, Guérin S, Guibout C, Shamsaldin A, Dondon MG, Valteau-Couanet D, Hartmann O, Hawkins M, de Vathaire F. Long-term risk of second malignant neoplasms after neuroblastoma in childhood: role of treatment. Int J Cancer. 2003;107(5):791-6.

Saarilahti K, Kouri M, Collan J, Kangasmäki A, Atula T, Joensuu H, Tenhunen M. Sparing of the submandibular glands by intensity modulated radiotherapy in the treatment of head and neck cancer. Radiother Oncol. 2006;78(3):270-5.

Salter BJ. NOMOS Peacock IMRT utilizing the Beak post collimation device. Med Dosim. 2001;26(1):37-45.

Sanchez-Nieto B, Nahum AE, Dearnaley DP. Individualization of dose prescription based on

normal-tissue dose-volume and radiosensitivity data. Int J Radiat Oncol Biol Phys. 2001;49(2):487-99.

Semenenko VA, Reitz B, Day E, Qi XS, Miften M, Li XA. Evaluation of a commercial biologically based IMRT treatment planning system. Med Phys. 2008;35(12):5851-60.

Sharma NK, Li T, Chen DY, Pollack A, Horwitz EM, Buyyounouski MK. Intensity-modulated radiotherapy reduces gastrointestinal toxicity in patients treated with androgen deprivation therapy for prostate cancer. Int J Radiat Oncol Biol Phys. 2011;80(2):437-44.

Shepard DM, Earl MA, Li XA, Naqvi S, Yu C. Direct aperture optimization: A turnkey solution for step-and-shoot IMRT. Med Phys. 2002;29(6):1007-18.

Siebers JV. The effect of statistical noise on IMRT plan quality and convergence for MC-based and MC-correction-based optimized treatment plans. J Phys Conf Ser. 2008;102:12020.

Siebers JV, Tong S, Lauterbach M, Wu Q, Mohan R. Acceleration of dose calculations for intensity-modulated radiotherapy. Med Phys. 2001;28(6):903-10.

Sikora M, Muzik J, Söhn M, Weinmann M, Alber M. Monte Carlo vs. pencil beam based optimization of stereotactic lung IMRT. Radiat Oncol. 2009;4:64.

Soret M, Bacharach SL, Buvat I. Partial-volume effect in PET tumor imaging. J Nucl Med. 2007;48(6):932-45.

South M, Chiu JK, Teh BS, Bloch C, Schroeder TM, Paulino AC. Supine craniospinal irradiation using intrafractional junction shifts and field-in-field dose shaping: early experience at Methodist Hospital. Int J Radiat Oncol Biol Phys. 2008;71(2):477-83.

South CP, Evans PM, Partridge M. Dose prescription complexity versus tumor control probability in biologically conformal radiotherapy. Med Phys. 2009;36(10):4379-88.

Søvik A, Malinen E, Skogmo HK, Bentzen SM, Bruland OS, Olsen DR. Radiotherapy adapted to spatial and temporal variability in tumor hypoxia. Int J Radiat Oncol Biol Phys. 2007a;68(5):1496-504.

Søvik A, Ovrum J, Olsen DR, Malinen E. On the parameter describing the generalised equivalent uniform dose (gEUD) for tumours. Phys Med. 2007b;23(3-4):100-6.

Speight JL, Roach M 3rd. Advances in the treatment of localized prostate cancer: the role of anatomic and functional imaging in men managed with radiotherapy. J Clin Oncol 2007;25(8):987-95.

Stavrev P, Hristov D, Warkentin B, Sham E, Stavreva N, Fallone BG. Inverse treatment planning by physically constrained minimization of a biological objective function. Med Phys. 2003;30(11):2948-58.

Stavreva NA, Warkentin B, Stavrev PV, Fallone BG. Investigating the effect of clonogen resensitization on the tumor response to fractionated external radiotherapy. Med Phys 2005;32:720-5.

Stewart AJ, Lee YK, Saran FH. Comparison of conventional radiotherapy and intensity-modulated radiotherapy for post-operative radiotherapy for primary extremity soft tissue sarcoma. Radiother Oncol. 2009;93(1):125-30.

Stewart RD, Li XA. BGRT: biologically guided radiation therapy-the future is fast approaching! Med Phys. 2007;34(10):3739-51.

Sze HC, Lee MC, Hung WM, Yau TK, Lee AW. RapidArc radiotherapy planning for prostate cancer: Single-arc and double-arc techniques vs. intensity-modulated radiotherapy. Med Dosim. 2012;37(1):87-91.

Söhn M, Yan D, Liang J, Meldolesi E, Vargas C, Alber M. Incidence of late rectal bleeding in high-dose conformal radiotherapy of prostate cancer using equivalent uniform dose-based and dose-volume-based normal tissue complication probability models. Int J Radiat Oncol Biol Phys. 2007;67(4):1066-73.

Tenhunen M, Usenius T, Lahtinen T. Irradiation of the whole neuraxis. A method for field positioning. Acta Oncol. 1994;33:661-5.

Teoh M, Clark CH, Wood K, Whitaker S, Nisbet A. Volumetric modulated arc therapy: a review of current literature and clinical use in practice. Br J Radiol. 2011;84(1007):967-96.

Tervo J, Kolmonen P. A model for the control of a multileaf collimator in radiation therapy treatment planning. Inv Probl. 2000;16:1875-95.

Tervo J, Kolmonen P, Lyyra-Laitinen T, Pinter JD, Lahtinen T. An optimization-based approach to the multiple static delivery technique in radiation therapy. Ann Oper Res. 2003;119:205-27.

Thorwarth D, Eschmann SM, Paulsen F, Alber M. Hypoxia dose painting by numbers: a planning study. Int J Radiat Oncol Biol Phys. 2007;68(1):291-300.

Tomé WA, Fowler JF. On cold spots in tumour subvolumes. Med Phys. 2002;29(7):1590–8.

Troost EG, Schinagl DA, Bussink J, Oyen WJ, Kaanders JH. Clinical evidence on PET-CT for radiation therapy planning in head and neck tumours. Radiother Oncol. 2010;96(3):328-34.

Tubiana M. Can we reduce the incidence of second primary malignancies occurring after radiotherapy? A critical review. Radiother Oncol. 2009;91(1):4-15.

Ulmer W, Pyyry J, Kaissl W. A 3D photon superposition/convolution algorithm and its foundation on results of Monte Carlo calculations. Phys Med Biol. 2005;50(8):1767-90.

van Asselen B, Schwarz M, van Vliet-Vroegindeweij C, Lebesque JV, Mijnheer BJ, Damen EM. Intensity-modulated radiotherapy of breast cancer using direct aperture optimization. Radiother Oncol. 2006;79(2):162-9.

van Battum LJ, Hoffmans D, Piersma H, Heukelom S. Accurate dosimetry with GafChromic EBT film of a 6 MV photon beam in water: what level is achievable? Med Phys. 2008;35(2):704-16.

Van Der Voort Van Zyp NC, Hoogeman MS, Van De Water S, Levendag PC, Van Der Holt B, Heijmen BJM, Nuyttens JJ. Clinical introduction of Monte Carlo treatment planning: a different prescription dose for non-small cell lung cancer according to tumour location and size. Radiother Oncol. 2010;96(1):55-60.

Van Esch A, Depuydt T, Huyskens DP. The use of an aSi-based EPID for routine absolute dosimetric pre-treatment verification of dynamic IMRT fields. Radiother Oncol. 2004;71(2):223-34.

Van Esch A, Tillikainen L, Pyykkonen J, Tenhunen M, Helminen H, Siljamäki S, Alakuijala J, Paiusco M, Lori M, Huyskens DP. Testing of the analytical anisotropic algorithm for photon dose calculation. Med Phys. 2006;33(11):4130-48.

van Lin EN, Fütterer JJ, Heijmink SW, van der Vight LP, Hoffmann AL, van Kollenburg P, Huisman HJ, Scheenen TW, Witjes JA, Leer JW, Barentsz JO, Visser AG. IMRT boost dose planning on dominant intraprostatic lesions: gold marker-based three-dimensional fusion of CT with dynamic contrast-enhanced and 1H-spectroscopic MRI. Int J Radiat Oncol Biol Phys. 2006;65(1):291-303.

Vanetti E, Clivio A, Nicolini G, Fogliata A, Ghosh-Laskar S, Agarwal JP, Upreti RR, Budrukkar A, Murthy V, Deshpande DD, Shrivastava SK, Dinshaw KA, Cozzi L. Volumetric modulated arc radiotherapy for carcinomas of the oro-pharynx, hypo-pharynx and larynx: a treatment planning comparison with fixed field IMRT. Radiother Oncol. 2009;92(1):111-7.

Vassiliev ON, Titt U, Pönisch F, Kry SF, Mohan R, Gillin MT. Dosimetric properties of photon beams from a flattening filter free clinical accelerator. Phys Med Biol. 2006;51(7):1907-1917.

Verbakel WF, Senan S, Cuijpers JP, Slotman BJ, Lagerwaard FJ. Rapid delivery of stereotactic radiotherapy for peripheral lung tumours using volumetric intensity-modulated arcs. Radiother Oncol. 2009;93(1):122-4.

Verellen D, Vanhavere F. Risk assessment of radiation-induced malignancies based on whole-body equivalent dose estimates for IMRT treatment in the head and neck region. Radiother Oncol. 1999;53(3):199-203.

Verellen D, Van den Heuvel F, De Neve W, De Beukeleer M, Storme G. Dynamic radiotherapy: interactive movement of patient couch for treatment of craniospinal axis. Int J Radiat Oncol Biol Phys. 1996;35(4):771-7.

Vergeer MR, Doornaert PA, Rietveld DH, Leemans CR, Slotman BJ, Langendijk JA. Intensity-modulated radiotherapy reduces radiation-induced morbidity and improves health-related quality of life: results of a nonrandomized prospective study using a standardized follow-up program. Int J Radiat Oncol Biol Phys. 2009;74(1):1-8.

Vial P, Greer PB, Hunt P, Oliver L, Baldock C. The impact of MLC transmitted radiation on EPID dosimetry for dynamic MLC beams. Med Phys. 2008;35(4):1267-77.

Vial P, Oliver L, Greer PB, Baldock C. An experimental investigation into the radiation field offset of a dynamic multileaf collimator. Phys Med Biol. 2006;51(21):5517-38.

Videtic GM, Stephans K, Reddy C, Gajdos S, Kolar M, Clouser E, Djemil T. Intensity-modulated radiotherapy-based stereotactic body radiotherapy for medically inoperable early-stage lung cancer: excellent local control. Int J Radiat Oncol Biol Phys. 2010;77(2):344-9.

Vieillot S, Azria D, Lemanski C, Moscardo CL, Gourgou S, Dubois JB, Aillères N, Fenoglietto P. Plan comparison of volumetric-modulated arc therapy (RapidArc) and conventional intensity-modulated radiation therapy (IMRT) in anal canal cancer. Radiat Oncol. 2010;5:92.

Wang JZ, Li XA, D'Souza WD, Stewart RD. Impact of prolonged fraction delivery times on tumor control: a note of caution for intensity-modulated radiation therapy (IMRT). Int J Radiat Oncol Biol Phys. 2003a;57(2):543-52.

Wang JZ, Guerrero M, Li XA. How low is the alpha/beta ratio for prostate cancer? Int J Radiat Oncol Biol Phys. 2003b;55(1):194-203.

Wiezorek T, Brachwitz T, Georg D, Blank E, Fotina I, Habl G, Kretschmer M, Lutters G, Salz H, Schubert K, Wagner D, Wendt TG. Rotational IMRT techniques compared to fixed gantry IMRT and tomotherapy: multi-institutional planning study for head-and-neck cases. Radiat Oncol. 2011;6:20.

Wilkens JJ, Alaly JR, Zakarian K, Thorstad WL, Deasy JO. IMRT treatment planning based on

prioritizing prescription goals. Phys Med Biol. 2007;52(6):1675-92.

Wilkinson JM, Lewis J, Lawrence GP, Lucraft HH, Murphy E. Craniospinal irradiation using a forward planned segmented field technique. Br J Radiol. 2007;80(951):209-15.

Witte M, Shakirin G, Houweling A, Peulen H, van Herk M. Dealing with geometric uncertainties in dose painting by numbers: introducing the ΔVH. Radiother Oncol. 2011;100(3):402-6.

Wu Q, Manning M, Schmidt-Ullrich R, Mohan R. The potential for sparing of parotids and escalation of biologically effective dose with intensity-modulated radiation treatments of head and neck cancers: a treatment design study. Int J Radiat Oncol Biol Phys. 2000a;46(1):195-205.

Wu Q, Arnfield M, Tong S, Wu Y, Mohan R. Dynamic splitting of large intensity-modulated fields. Phys Med Biol. 2000b;45(7):1731-40.

Wu Q, Mohan R, Niemierko A, Schmidt-Ullrich R. Optimization of intensity-modulated radiotherapy plans based on the equivalent uniform dose. Int J Radiat Oncol Biol Phys. 2002;52(1):224-35.

Wu QJ, Yoo S, Kirkpatrick JP, Thongphiew D, Yin FF. Volumetric arc intensity-modulated therapy for spine body radiotherapy: comparison with static intensity-modulated treatment. Int J Radiat Oncol Biol Phys. 2009;75(5):1596-604.

Wu SW, Chao TC, Tung CJ, Lin MH, Lee CC. MLC mediated beam hardening effects in IMRT. Radiat Meas. 2011;46(12):1989-92.

Xu XG, Bednarz B, Paganetti H. A review of dosimetry studies on external-beam radiation treatment with respect to second cancer induction. Phys Med Biol. 2008;53(13):R193-241.

Yom SS, Frija EK, Mahajan A, Chang E, Klein K, Shiu A, Ohrt J, Woo S. Field-in-field technique with intrafractionally modulated junction shifts for craniospinal irradiation. Int J Radiat Oncol Biol Phys. 2007;69(4):1193-8.

Yoo S, Wu QJ, Lee WR, Yin FF. Radiotherapy treatment plans with RapidArc for prostate cancer involving seminal vesicles and lymph nodes. Int J Radiat Oncol Biol Phys. 2010;76(3):935-42.

Yorke ED, Kutcher GJ, Jackson A, Ling CC. Probability of radiation-induced complications in normal tissues with parallel architecture under conditions of uniform whole or partial organ irradiation. Radiother Oncol. 1993;26(3):226-37.

Yu CX. Intensity-modulated arc therapy with dynamic multileaf collimation: an alternative to tomotherapy. Phys Med Biol. 1995;40(9):1435-49.

Zaider M, Minerbo GN. Tumour control probability: A formulation applicable to any temporal protocol of dose delivery. Phys Med Biol. 2000;45(2):279–93.

Zelefsky MJ, Fuks Z, Happersett L, Lee HJ, Ling CC, Burman CM, Hunt M, Wolfe T, Venkatraman ES, Jackson A, Skwarchuk M, Leibel SA. Clinical experience with intensity modulated radiation therapy (IMRT) in prostate cancer. Radiother Oncol. 2000;55(3):241-9.

Zelefsky MJ, Fuks Z, Hunt M, Yamada Y, Marion C, Ling CC, Amols H, Venkatraman ES, Leibel SA. High-dose intensity modulated radiation therapy for prostate cancer: early toxicity and biochemical outcome in 772 patients. Int J Radiat Oncol Biol Phys. 2002;53(5):1111-6.

Zelefsky MJ, Yamada Y, Fuks Z, Zhang Z, Hunt M, Cahlon O, Park J, Shippy A. Long-term results of conformal radiotherapy for prostate cancer: impact of dose escalation on biochemical tumor control and distant metastases-free survival outcomes. Int J Radiat Oncol Biol Phys. 2008a;71(4):1028-33.

Zelefsky MJ, Levin EJ, Hunt M, Yamada Y, Shippy AM, Jackson A, Amols HI. Incidence of late rectal and urinary toxicities after three-dimensional conformal radiotherapy and intensity-modulated radiotherapy for localized prostate cancer. Int J Radiat Oncol Biol Phys. 2008b;70(4):1124-1129.

Zietman AL, DeSilvio ML, Slater JD, Rossi CJ Jr, Miller DW, Adams JA, Shipley WU. Comparison of conventional-dose vs high-dose conformal radiation therapy in clinically localized adenocarcinoma of the prostate: a randomized controlled trial. JAMA. 2005;294(10):1233-9.

Zhang X, Liu H, Wang X, Dong L, Wu Q, Mohan R. Speed and convergence properties of gradient algorithms for optimization of IMRT. Med Phys. 2004;31(5):1141-52.

Zhang X, Wang X, Dong L, Liu H, Mohan R. A sensitivity-guided algorithm for automated determination of IMRT objective function parameters. Med Phys. 2006;33(8):2935-44.

Zygmanski P, Kung JH. Method of identifying dynamic multileaf collimator irradiation that is highly sensitive to a systematic MLC calibration error. Med Phys. 2001;28(11):2220-6.

Zygmanski P, Rosca F, Kadam D, Lrenz F, Nalichowski A, Chin L. Determination of depth and field size dependence of multileaf collimator transmission in intensity-modulated radiation therapy beams. J Appl Clin Med Phys. 2007;8(4):76-95.

Ågren A, Brahme A, Turesson I. Optimization of uncomplicated control for head and neck tumors. Int J Radiat Oncol Biol Phys 1990;19(4):1077-85.